Acta Pharmaceutica Sinica B 2025;15(9):4751−4771

Chinese Pharmaceutical Association
Institute of Materia Medica, Chinese Academy of Medical Sciences

Acta Pharmaceutica Sinica B

www.elsevier.com/locate/apsb
www.sciencedirect.com

ORIGINAL ARTICLE

USP20 as a super-enhancer-regulated gene drives T-ALL progression *via* HIF1A deubiquitination

Ling Xu[a,b,†], Zimu Zhang[c,†], Juanjuan Yu[a,†], Tongting Ji[a,†], Jia Cheng[a,†], Xiaodong Fei[d,†], Xinran Chu[e], Yanfang Tao[f], Yan Xu[b], Pengju Yang[a], Wenyuan Liu[g], Gen Li[c], Yongping Zhang[e], Yan Li[b], Fenli Zhang[h], Ying Yang[h], Bi Zhou[a,i], Yumeng Wu[a,j], Zhongling Wei[e], Yanling Chen[a], Jianwei Wang[c], Di Wu[c], Xiaolu Li[c], Yang Yang[c], Guanghui Qian[c], Hongli Yin[c], Shuiyan Wu[e], Shuqi Zhang[k], Dan Liu[l], Jun-jie Fan[e], Lei Shi[m], Xiaodong Wang[n], Shaoyan Hu[e,*], Jun Lu[e,*], Jian Pan[c,*]

[a]*Children's Hospital of Soochow University, Suzhou 215003, China*
[b]*Department of Pediatrics, the Affiliated Hospital of Xuzhou Medical University, Xuzhou 221000 China*
[c]*Institute of Pediatric Research, Children's Hospital of Soochow University, Suzhou 215003, China*
[d]*Department of Radiology, Children's Hospital of Soochow University, Suzhou 215003, China*
[e]*Department of Hematology, Children's Hospital of Soochow University, Suzhou 215003, China*
[f]*Department of Traditional Chinese Medicine, Children's Hospital of Soochow University, Suzhou 215003, China*
[g]*Department of Pediatrics, the Second Affiliated Hospital of Anhui Medical University, Hefei 230601, China*
[h]*Clinical Medicine, Guizhou Medical University, Guiyang 550000, China*
[i]*Department of Pediatric, Suzhou Hospital of AnHui Medical University, Suzhou 234000, China*
[j]*Department of Pediatric, the First Affiliated Hospital of Bengbu Medical College, Bengbu 233004, China*
[k]*Department of Pediatrics, the First Affiliated Hospital of Wannan Medical College, Wuhu 241002, China*
[l]*Department of Blood Transfusion, Children's Hospital of Soochow University, Suzhou 215003, China*
[m]*Department of Medicinal Chemistry, Jiangsu Key Laboratory of Drug Design and Optimization, China Pharmaceutical University, Nanjing 210009, China*
[n]*Department of Orthopaedics, Children's Hospital of Soochow University, Suzhou 215003, China*

Received 12 November 2024; received in revised form 4 March 2025; accepted 9 March 2025

*Corresponding authors.
E-mail addresses: panjian2008@163.com (Jian Pan), drlujun_sz@163.com (Jun Lu), hsy139@126.com (Shaoyan Hu).
[†]These authors made equal contributions to this work.

Peer review under the responsibility of Chinese Pharmaceutical Association and Institute of Materia Medica, Chinese Academy of Medical Sciences.

https://doi.org/10.1016/j.apsb.2025.07.003

KEY WORDS

T-ALL;
Super enhancer;
USP20;
HIF1A;
GSK2643943A;
H3K27ac ChIP-seq;
Transcription regulation;
Potential target

Abstract T-cell acute lymphoblastic leukemia (T-ALL) is a highly aggressive hematologic malignancy with a poor prognosis, despite advancements in treatment. Many patients struggle with relapse or refractory disease. Investigating the role of the super-enhancer (SE) regulated gene ubiquitin-specific protease 20 (*USP20*) in T-ALL could enhance targeted therapies and improve clinical outcomes. Analysis of histone H3 lysine 27 acetylation (H3K27ac) chromatin immunoprecipitation sequencing (ChIP-seq) data from six T-ALL cell lines and seven pediatric samples identified *USP20* as an SE-regulated driver gene. Utilizing the Cancer Cell Line Encyclopedia (CCLE) and BloodSpot databases, it was found that *USP20* is specifically highly expressed in T-ALL. Knocking down *USP20* with short hairpin RNA (shRNA) increased apoptosis and inhibited proliferation in T-ALL cells. *In vivo* studies showed that *USP20* knockdown reduced tumor growth and improved survival. The USP20 inhibitor GSK2643943A demonstrated similar anti-tumor effects. Mass spectrometry, RNA-Seq, and immunoprecipitation revealed that USP20 interacted with hypoxia-inducible factor 1 subunit alpha (HIF1A) and stabilized it by deubiquitination. Cleavage under targets and tagmentation (CUT&Tag) results indicated that USP20 co-localized with HIF1A, jointly modulating target genes in T-ALL. This study identifies USP20 as a therapeutic target in T-ALL and suggests GSK2643943A as a potential treatment strategy.

1. Introduction

T-ALL is a highly aggressive form of leukemia characterized by the clonal proliferation of abnormal T lymphocytes. It accounts for approximately 15%[1] of ALL cases in children and 25% in adults[2]. T-ALL presents greater clinical challenges than B-cell acute lymphoblastic leukemia due to its poor treatment response, higher relapse rates, increased risk of progression to refractory leukemia, and a long-term survival rate of less than 10%[3]. Therefore, studying the pathogenesis of T-ALL may provide crucial insights for developing targeted therapies essential for improving clinical outcomes.

Recent studies have highlighted the pivotal role of deubiquitinating enzymes (DUBs) in tumor progression. Among the various subfamilies of DUBs, ubiquitin-specific peptidases (USPs) are the largest and have been found to be involved in tumor progression[4]. USP7, one of the earliest identified DUBs in T-ALL, stabilizes the tumor suppressor protein p53 by removing ubiquitin (Ub) chains, enhancing its anticancer function[5]. USP7 also regulates various oncogenes, such as *Notch1*, by deubiquitination, thus promoting their stability and influencing the Notch signaling pathway, which enhances T-ALL cell proliferation[6]. This dual role positions USP7 as a potential therapeutic target. Additionally, *USP1* is aberrantly expressed in T-ALL and is essential for its survival, with the USP1/PLK1/LDHA axis playing a significant role in glycolysis and disease progression[7]. USP44, by interacting with WD repeat domain 5 (WDR5), inhibits its ubiquitination, thereby promoting T-ALL growth[8]. Further investigation into the mechanisms by which DUBs contribute to T-ALL will inform the discovery of novel targeted treatments, a vital step toward better therapeutic efficacy.

In 2013, Young's lab introduced the concept of SEs, highly active enhancers enriched with transcription factors (TFs), cofactors, and histone modifications[9], such as H3K27ac, a marker for SEs[10]. SEs exhibit higher activity than normal enhancers and play a crucial role in cell-specific gene expression and differentiation, impacting tumor cell phenotype and function[11,12]. SEs have been closely linked to the development of various cancers, such as pancreatic cancer, where they regulate transforming growth factor beta receptor 2 expression, impacting transforming growth factor beta signaling[13]. In breast cancer, the loss of H3K27ac-SEs contributes to its tissue-specific tumor-suppressive functions[14]. In colorectal cancer, SEs drive the activation of the homeobox B cluster (*HOXB*) gene cluster, particularly the oncogene *HOXB8*, influencing prognosis[15]. SEs also regulate key transcription factors in esophageal adenocarcinoma, such as E74-like ETS transcription factor 3, krüppel-like factor 5, GATA binding protein 6, and ETS homologous factor, enhancing esophageal adenocarcinoma cell proliferation and survival[16]. SEs also play key roles in hepatocellular carcinoma[17], multiple myeloma[18], and B-cell acute lymphoblastic leukemia[19]. Our previous studies revealed that SE-associated tetratricopeptide repeat domain 8 (TTC8) in neuroblastoma (NB) altered paired-like homeobox 2B distribution and activated mitogen-activated protein kinase (MAPK) signaling, promoting tumorigenesis[20]. The bromodomain-containing protein 4 (BRD4) inhibitor GNE987, targeting SEs, demonstrated anticancer effects in NB[21]. The identification of hub genes driven by SEs has attracted significant research interest due to their association with various cancers, presenting potential therapeutic targets.

In leukemia, Sanda's group[22-24] conducted enhancer analysis on primary leukemic samples from adult T-cell leukemia/lymphoma (ATL) and identified several oncogenes associated with SEs, such as T-cell lymphoma invasion and metastasis 2, interferon regulatory factor 4 (*IRF4*), nuclear factor kappa-light-chain-enhancer of activated B cells (*NF-kB)*, and tumor protein p73 (*TP73*), which promote ATL progression. Mansour et al.[25] discovered a mutation upstream of the T-cell acute lymphocytic leukemia protein 1 (*TAL1*) gene's transcription start site that generates a super enhancer, leading to overexpression of the oncogene and promoting T-ALL development. Smith et al.[26] found that mebendazole targets the myeloblastosis oncogene (*MYB*)-dependent oncogene TAL1 5′SE, inducing MYB protein degradation and T-ALL cell death. These findings underscore the

critical role of SEs in leukemia pathogenesis. Our previous research, using H3K27ac ChIP-seq data from acute myeloid leukemia (AML) clinical samples and cell lines, identified SE-regulated oncogenes, such as acidic nuclear phosphoprotein 32 family member B (*ANP32B)*, which enhances v-myc avian myelocytomatosis viral oncogene homolog (*MYC)* through histone acetylation, promoting AML proliferation[27]. Down-regulation of SE-associated genes, including lymphoblastic leukemia-derived sequence 1 (*LYL1*), was observed following GNE-987 treatment[28]. Our previous study revealed that the BRD4 inhibitor GNE-987 effectively inhibits T-ALL progression by targeting SE-related genes[29] and highlights the high expression and crucial role of the SE-regulated gene FYN binding protein 1 in T-ALL[30]. Therefore, investigating SE-regulated genes in T-ALL is essential for understanding its molecular mechanisms and developing targeted therapies.

This study screened the DUB family based on H3K27ac ChIP-seq data from pediatric clinical samples and T-ALL cells, identifying USP20 as an SE-regulated DUB in T-ALL. It has been shown to deubiquitinate proteins, such as D2, HIF1A, and β2-AR, thereby influencing important cellular processes, including Wnt signaling, HIF1A signaling, NF-κB signaling, tumorigenesis, and tumor progression[31]. *USP20* is often detrimental in cancer therapy and overexpressed in various tumors. Recent studies have revealed its significant role in the tumorigenesis of breast cancer, colon cancer, lung cancer, gastric cancer, and ATL[4]. Specific inhibition of USP20 activity presents a promising approach for novel tumor therapy. For instance, the small molecule inhibitor GSK2643943A has demonstrated its ability to inhibit USP20's deubiquitinating activity[32]. However, the specific mechanism of USP20 in T-ALL remains unknown. Our study uncovered that knocking down *USP20* using shRNA increased T-ALL cell apoptosis and inhibited cell proliferation. *In vivo*, *USP20* knockdown reduced tumor growth and prolonged survival in mice. The USP20 inhibitor GSK2643943A exhibits similar antitumor effects. Our findings deepen the understanding of T-ALL's basic biology and clinical features and propose a potential new therapeutic strategy, making USP20 a promising target in T-ALL treatment and offering new directions for future clinical interventions.

2. Methods and materials

2.1. Cell culture

Shanghai Zhong Qiao Xin Zhou Biotechnology Co., Ltd. supplied the J.gamma1, 6T-CEM, MOLT-4, and Jurkat human leukemia cell lines. HUT78 and CCRF-CEM came from the Chinese Academy of Sciences Cell Bank. Complete RPMI 1640 media (VivaCell, Shanghai, China) supplemented with 10% FBS (Biological Industries, CT, USA) was used to cultivate these cells. HEK293FT cells were obtained from the Cell Bank of the Chinese Academy of Sciences and maintained in DMEM (VivaCell, Shanghai, China) supplemented with 10% fetal bovine serum (Biological Industries, CT, USA). All cell lines underwent authentication by STR analysis and testing for mycoplasma using the MycoAlert kit.

2.2. Lentivirus generation and infection

IGE Biotechnology LTD in China synthesized and integrated shRNA into the pLKO.1 vector, with the sequences provided in Supporting Information Table S1. A total of 15 μg, consisting of target and packaging plasmids (psPAX2: #12260; pMD2.G: #12259) in a 4:3:1 ratio, was transfected into 293FT cells using PEI reagent. Six hours later, the medium was replaced with fresh DMEM, and the virus suspension was collected after 48 h and subsequently filtered. T-ALL cells were exposed to lentivirus with 1 μg/mL Polybrene for 24 h. Stable T-ALL cell lines were established by selection with 1 μg/mL puromycin (ST551). For *USP20* overexpression, the Flag-tagged *USP20* CDS was cloned into pLVX-EF1α-IRES-puro. HEK293FT cells were transfected with target and packaging plasmids (a total of 15 μg, in a ratio of 2:2:1) using a PEI reagent. Lentivirus was utilized to infect T-ALL cells, resulting in the acquisition of *USP20*-overexpressing T-ALL cell lines after puromycin selection. Overexpression of *HIF1A*, catenin beta 1 (*CTNNB1)*, runt-related transcription factor 1 (*RUNX1),* and ETS proto-oncogene 1 (*ETS1)* was also obtained by lentiviral transduction.

2.3. CRISPR-mediated silencing of USP20

To establish stable knockout cell lines using the dCas9/CRISPR system, Jurkat and J.gamma1 cells were initially transfected with lentiviruses containing the dCas9 gene and subsequently subjected to puromycin selection. Subsequently, small guide RNAs (sgRNAs) targeting *USP20* were cloned into a Lenti-CRISPR plasmid synthesized by IGE Biotechnology LTD (Guangzhou, China). The dCas9-expressing cells were subsequently transduced with either sgRNA-*USP20* or non-targeted control sgRNA (sg-NC) lentiviral particles. The preparation of the lentiviral particles was conducted by IGE Biotechnology LTD (Guangzhou, China) following a previously described method, and the target sequence information is provided in Supporting Information Table S2.

2.4. RNA purification, cDNA generation, and qRT-PCR

FastPure Cell/Tissue Total RNA Isolation Kit V2 (Vazyme, Nanjing, China) was used to extract total RNA. Subsequently, the High-Capacity cDNA Reverse Transcription Kit (Applied Biosystems, Waltham, MA, USA) was used to reverse transcribe 2 μg of total RNA into cDNA. The LightCycler® 480 SYBR® Green I Master Mix on a LightCycler® 480 Real-Time System (Roche, Grunzak, Germany) was used for quantitative real-time polymerase chain reaction (qRT-PCR). The $2^{-\Delta\Delta CT}$ technique was used to quantify relative gene expression, normalizing Ct values to GAPDH. Gene expression was averaged from three replicates. Supporting Information Table S3 lists primer sequences.

2.5. Western blotting analysis

The following antibodies were used: USP20 (Proteintech, 17491-1-AP, Wuhan, China), β-actin (Proteintech, 66009-1-Ig, Wuhan, China), PARP (CST, 9542S, Danvers, USA), cleaved caspase-3 (CST, 9661S, Danvers, USA), cleaved caspase-8 (CST, 9746S, Danvers, USA); c-Myc (CST, 9402S, Danvers, USA); Flag (Sigma, F1804, St. Louis, MO, USA), HIF1A (Santa Cruz Biotechnology, sc-3515, Dallas, TX, USA), HA-Tag (CST, 3724S, Danvers, USA), IgG (Abcam, ab172730, Cambridge, MA, USA), β-Catenin (CST, 9582S, Danvers, USA), GFP (Proteintech, 66002-1-Ig, Wuhan, China), GAPDH (Abcam, ab128915,

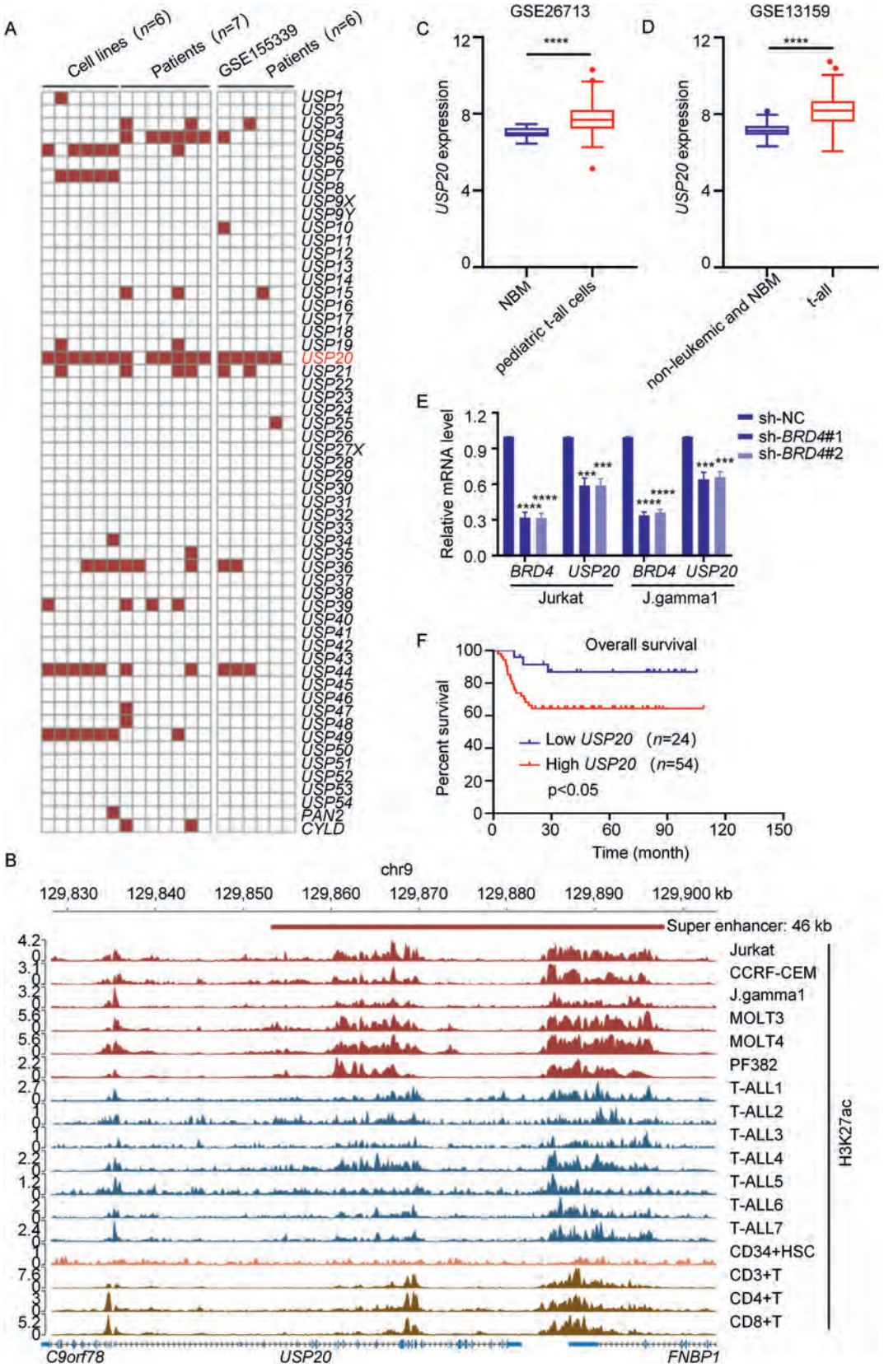

Figure 1 Identification of the T-ALL SE regulatory gene *USP20*, which exhibits high expression in T-ALL and correlates with poor prognosis. (A) H3K27ac ChIP-seq analysis of six T-ALL cell lines and seven patients with T-ALL, as well as data from six patients with T-ALL from the GEO dataset, were analyzed to screen for potential super-enhancer (SE) driver genes in the USP family. (B) An enrichment near *USP20* was identified, indicating a high likelihood of super-enhancers. This was observed when comparing the H3K27ac ChIP-seq results from our six T-ALL

Cambridge, MA, USA), LDB1 (Abcam, ab96799, Cambridge, MA, USA), BRD4 (E2A7X) Rabbit mAb (CST, 13440, Danvers, USA).

2.6. Cell proliferation experiment

Infected cells from the experimental and control groups were seeded at 3×10^3 per well into 96-well plates following puromycin screening. Proliferation was evaluated using the Cell Counting Kit-8 (APExBIO, K1018-1, Houston, USA) by adding CCK-8 reagent to each well on Days 1, 3, and 5. Absorbance at 450 nm was measured using a spectrometer (Thermo, Waltham, MA, USA) to determine cell activity. To determine the IC_{50} of GSK2643943A, cells were treated with GSK2643943A (30 nmol/L−4 μmol/L), for 24 h at a density of 1×10^4 cells per well, with each concentration replicated at least three times per cell line.

2.7. Soft agar clone formation assay

The bottom gel was prepared using 1.2% agarose gel and 2 × RPMI 1640 (YuChun, YC-1010, Shanghai, China) with 20% FBS. Following solidification, 100 μL of cell suspension from sh-NC and sh-*USP20* groups was added to the soft agar medium in 6-well plates (5×10^3 cells/mL). The upper gel consisted of 0.7% agarose gel with 2 × RPMI 1640 and 20% bovine serum. Plates were then incubated at 37 °C with CO_2 for about 14 days, followed by fixation with 4% paraformaldehyde (Beyotime, P0099, Shanghai, China) for 24 h, staining with Giemsa (Beyotime, C0131, Shanghai, China), and subsequent colony counting.

2.8. Cell apoptosis assay

After puromycin selection, the infected cells were washed with cold 1 × PBS. Subsequently, the samples were resuspended in 1 × Annexin V binding buffer and labeled with FITC-Annexin V antibody and PI solution according to the instructions provided in the FITC-Annexin V apoptosis kit manual (BD Biosciences, 556547, San Jose, CA, USA). Cell apoptosis was evaluated using the Beckman Gallios™ Flow Cytometer (Beckman, Krefeld, Germany).

2.9. Luciferase reporter assay

The *USP20*-SE candidate enhancer was divided into three components, E1−E3 (Supporting Information Table S4). Candidate enhancer constituents in the *USP20*-SE were cloned into the luciferase reporter vector pGL3-Promoter (Promega, Madison, WI, USA). The vectors were transfected into the J.gamma1 cell line using Lipofectamine 3000 (Thermo Fisher Scientific, L3000001, Waltham, MA, USA). A Renilla luciferase control vector was co-transfected to enable normalization. Luciferase activity was assessed 48 h post-transfection using the Dual-Luciferase Reporter Assay System (Promega, E1910, Madison, WI, USA).

2.10. Cell cycle analysis

Cells were harvested, washed with cold PBS, and then fixed in 70% ethanol overnight. Subsequently, cell cycle analysis was performed according to the manufacturer's protocol using the "Cell Cycle and Apoptosis Analysis Kit" (Beyotime, C1052, Shanghai, China). Flow cytometry (Beckman Gallios™ Flow Cytometer) (Beckman, Krefeld, Germany) was utilized to determine the distribution of cells in different phases of the cell cycle.

2.11. RNA sequencing and data processing

BGI Tech Service Co., Ltd. (Shenzhen, China) isolated the RNAs, prepared the library, sequenced the transcripts, and filtered the data. The 150 bp paired-end reads were aligned to the hg38 genome (Ensembl) employing HISAT2 software (version 2.2.0). StringTie software (version 2.1.2) was utilized for transcriptome assembly and abundance analysis. Differentially expressed genes were detected using the R/Bioconductor package DESeq2. Gene set enrichment analysis (GSEA) was performed using the R/Bioconductor package clusterProfiler, utilizing Hallmarks gene sets sourced from the Molecular Signatures Database (MSigDB).

2.12. In vivo experiments

All animal studies were approved by the Animal Care Committee of Suzhou College (approval number: CAM-SU-AP#: JP-2018-1). Female NSG mice aged 5 weeks (Shanghai Model Organisms Center, Inc., Shanghai, China) were randomly separated into two groups ($n > 6$ per group) to test USP20 function *in vivo*. The tail vein was infused with 2×10^6 J.gamma1 cells expressing firefly luciferin and either Sh-NC or Sh-USP20 in 100 μL PBS for each animal. On Days 0, 19, 29, 36, and 43 post-injection, tumor-bearing animals received 50 mg/kg intraperitoneal D-fluorescein sodium salt (GoldBio, 115144-35-9, St. Louis, MO, USA). IVIS (In Vivo Imaging Systems) imaging measured tumor radiance uptake utilizing Berthold imaging equipment (Berthold Technologies GmbH & Co. KG, Bad Wildbad, Germany). After CO_2 inhalation, mice were sacrificed, and liver, splenic, and bone tissues were taken for flow cytometry analysis with CD45 detection, paraffin embedding, hematoxylin and eosin (H&E) staining, and immunohistochemistry (IHC). To research GSK2643943A *in vivo*, NSG mice were randomly split into two groups ($n > 6$ per group). The tail vein of each mouse received an injection of 2×10^6 J.gamma1 cells expressing firefly luciferin (100 μL PBS). On Days 0 and 10 post-injection, D-fluorescein sodium salt was intraperitoneally injected for fluorescence imaging. Two days later, the experimental group received intraperitoneal injections of 15 mg/kg GSK2643943A while the control group received 15 mg/kg 5%®

cell lines, seven patients with T-ALL, and T cells from the GEO dataset using the IGV visualization tool. However, no enrichment near *USP20* was observed in the H3K27ac ChIP-seq data of $CD34^+$ HSC from the GEO dataset. (C) Data from the GEO dataset GSE26713 revealed significantly higher mRNA expression of *USP20* in patients with T-ALL ($n = 117$) than in bone marrow samples ($n = 7$) from healthy donors. (D) Data from the GEO dataset GSE13159 also showed significantly higher mRNA expression of *USP20* in T-ALL ($n = 165$) than bone marrow samples from non-leukemic individuals and healthy bone marrow ($n = 71$). (E) Knockdown of *BRD4* in T-ALL cells resulted in decreased expression of *USP20* mRNA levels ($n = 3$). (F) Our center's clinical data showed that survival rates were lower for individuals with T-ALL who expressed higher levels of USP20. Data are presented as mean ± SD; non-significant (ns), $^*P < 0.05$, $^{**}P < 0.01$, $^{***}P < 0.001$, and $^{****}P < 0.0001$.

HS15 (solvent for GSK2643943A), once daily for 10 times (with a 2-day interval). Imaging continued on Days 16, 23, 29, and 36 using the Berthold imaging system. Liver, spleen, bone, renal, and intestinal samples were harvested for further analysis.

2.13. CUT&Tag assay and data processing

CUT&Tag assays were conducted using the Hyperactive Universal CUT&Tag Assay Kit for Illumina (Vazyme, TD903, Nanjing, China) following the manufacturer's instructions. Antibodies against IgG, USP20, and HIF1A were employed. DNA was extracted and amplified with i5 and i7 primers in TruePrep Index Kit V2 for Illumina (Vazyme, TD202, Nanjing, China). Libraries were purified with VAHTS DNA Clean Beads (Vazyme, N411, Nanjing, China) and sequenced by Novogene Bioinformatics Technology Co., Ltd. (Beijing, China). The 150 bp paired-end reads were aligned to the hg38 (Ensembl) genome using Bowtie2 (version 2.4.4) with parameters –end-to-end– very-sensitive –no-mixed –no-discordant. Duplicates were removed using Picard tools. Peaks were called using MACS (version 3.0).

2.14. Immunoprecipitation

Jurkat and J.gamma1 cells transfected with *USP20*-Flag overexpression constructs were lysed using NP-40 lysis buffer (Beyotime, P0013F, Shanghai, China) and protein inhibitor. After incubation for half an hour at 4 °C, the samples were centrifuged, and the upper layer was extracted. A portion of the supernatant was denatured with a loading buffer and used as input. The remaining supernatant was incubated with Protein A/G beads along with either Flag or IgG antibodies overnight at 4 °C. Subsequently, the samples were centrifuged, and the pellets were washed with TBST before being subjected to mass spectrometry analysis or resuspended in loading buffer for Western blot. For the co-immunoprecipitation experiment on 293FT cells transfected with plasmids, Beaver Bio's Protein A/G IP kit was utilized. The process involved cell lysis, collection of supernatant, magnetic bead pretreatment, antibody binding, and antigen precipitation. Antigen elution was performed using a loading buffer, followed by magnetic separation and collection for Western blot analysis.

2.15. Human tissue samples, ChIP-seq, and SE analysis

This research was authorized by the Human Care Committee of Soochow University (approval number: 2023CS106). Written informed consent was obtained from all patients' legal guardians. Bone marrow samples from newly diagnosed pediatric T-ALL patients underwent ChIP assays following standard procedures[28]. Cells were fixed, lysed, and fragmented into chromatin pieces ranging from 300 to 800 bp. The chromatin was then incubated with an H3K27ac antibody, and the resulting antibody−chromatin complexes were isolated and purified. DNA sequencing was performed by BGI, with alignment to the hg38 genome reference. Super enhancers were identified using the ROSE software. Our sequencing and processed data files were submitted to the Gene Expression Omnibus (GEO; http://www.ncbi.nlm.nih.gov/geo/) repository, GSE267758 (T-ALL1, T-ALL2, T-ALL3, T-ALL4, T-ALL5, T-ALL6, T-ALL7, and J.gamma1 ChIP-seq), GSE165207 (T-ALL Hi-ChIP).

2.16. Statistical analysis

Results from various experiments were reported as the average value plus or minus the standard error of the mean. The statistical analysis involved the use of two-tailed, unpaired Student's *t*-tests for comparing two groups, and one-way analysis of variance (ANOVA) followed by Sidak's multiple comparison test for assessing numerous groups. "NS" denotes non-significant. $P < 0.05$ was regarded as statistically significant: $^{*}P < 0.05$, $^{**}P < 0.01$, $^{***}P < 0.001$, and $^{****}P < 0.0001$. We performed GraphPad Prism 8.0 software (GraphPad Software Inc., La Jolla, CA, USA) for all statistical analyses.

Additional methodological details can be found in the Supporting Information (Supporting Information and Methods section).

3. Results

3.1. Identification of USP20 as an SE-regulated gene in T-ALL, associated with high expression and poor prognosis

To identify genes associated with SEs in T-ALL, we analyzed H3K27ac ChIP-seq data from six T-ALL cell lines (Jurkat, J.gamma1, CCRF, MOLT3, MOLT4, PF382) (Supporting Information Table S5) and seven patients with T-ALL (Supporting Information Tables S6 and S7). Using ROSE software, we mapped the SE landscape across these 13 samples. Among the USP family genes, *USP4*, *USP5*, *USP7*, *USP20*, *USP36*, *USP44*, and *USP49* were found to overlap with or be flanked by SEs in multiple samples (Fig. 1A, Supporting Information Figs. S1 and S2). Further analysis of six H3K27ac ChIP-seq samples from patients with T-ALL in the GEO dataset GSE155339 supported *USP20* as an SE-driven gene (Fig. 1A). Notably, *USP20* was recognized as a potential SE-driven gene in over 90% of the samples. Consistent patterns were observed at the *USP20* locus in six T-ALL cell lines, seven patients with T-ALL, and three T-cell samples (GSE18927), but not in CD34+ HSC (GSE231486) (Fig. 1B). Data from the GEO dataset GSE26713 revealed that patients with T-ALL exhibited significantly higher *USP*20 mRNA expression than normal bone marrow (NBM) (Fig. 1C). Additionally, data from GSE13159 demonstrated that *USP*20 mRNA expression was notably elevated in patients with T-ALL compared to bone marrow samples from non-leukemic and healthy individuals (Fig. 1D). Analysis of the CCLE database indicated that *USP*20 mRNA expression levels ranked the highest among T-ALL cell lines compared to other cancer types (Supporting Information Fig. S3A). BloodSpot data also confirmed high expression of *USP20* in T-ALL (Fig. S3B), suggesting a significant role for *USP20* due to its specific high expression in T-ALL. To establish the specificity of sh*BRD4*'s effects, we measured the mRNA levels of *USP20*, *USP44*, and other non-SE-driven USP family members (Supporting Information Fig. S4A). Following *BRD4* knockdown in T-ALL cells, the *USP*20 mRNA and USP20 protein levels were reduced (Fig. 1E and Fig. S4B), with similar results observed using a BRD4 inhibitor (GNE987), indicating regulation of *USP*20 by SEs (Fig. S4C).

Cyclin-dependent kinase 7 (CDK7) is also a marker of SE. Applying CDK7 inhibitor (CDK7-IN-4) in T-ALL cells resulted in decreased expression of *USP*20 mRNA levels (Fig. S4D). Western blot analysis revealed high levels of USP20 in peripheral blood T lymphocytes of children with T-ALL and T-ALL cell lines

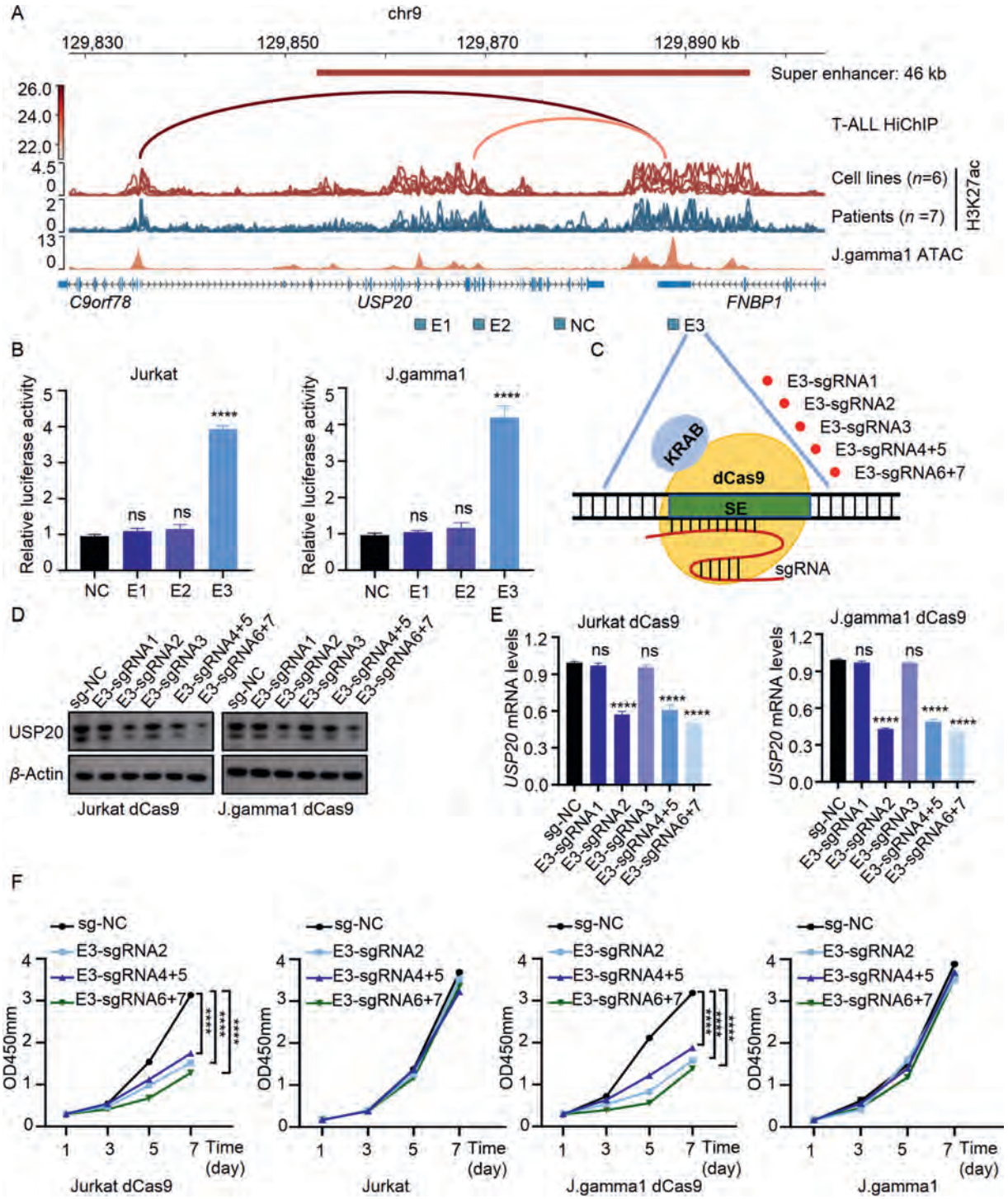

Figure 2 Regulation of USP20 by related super enhancers. (A) The ChIP-seq gene location reflected the ATAC and H3K27ac signals at the *USP20* gene location. The figure shows the Hi−C interaction in T-ALL, labeling three candidate enhancer regions (E1, E2, and E3) for *USP20*. (B) The study evaluated the transfection efficiency of Jurkat and J.gamma1 cells with the dual-luciferase reporter carrier incorporating NC or *USP20*-enhancer components ($n = 3$). (C) A schematic demonstrates the use of dead Cas9 fused to a transcriptional repressor domain (KRAB) to inhibit constitutive enhancers of *USP20*. (D) Western blot results of Jurkat and J.gamma1 cells after transfection with sgRNA-dCas9 vectors are presented. (E) The mRNA expression levels of *USP20* in Jurkat and J.gamma1 cells after transfection with sgRNA-dCas9 vectors are shown ($n = 3$). (F) CCK8 assays were used to evaluate the survival rate of Jurkat dCas9, Jurkat, J.gamma1 dCas9, and J.gamma1 cells upon transfection with non-targeting negative control and E3-targeting sgRNAs to assess cellular viability ($n = 3$). Data are presented as mean ± SD; non-significant (ns), $^{*}P < 0.05$, $^{**}P < 0.01$, $^{***}P < 0.001$, and $^{****}P < 0.0001$.

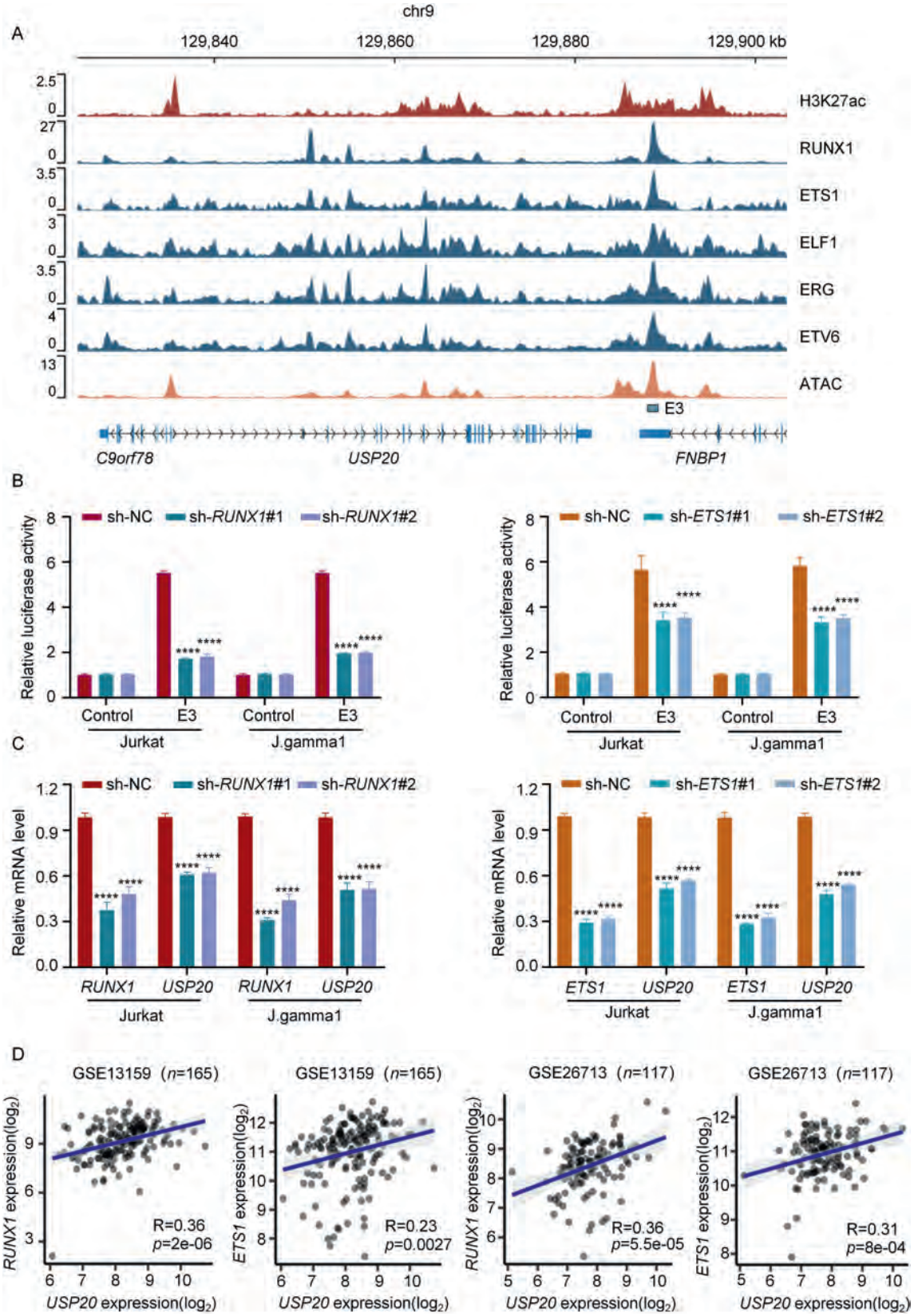

Figure 3 The pivotal role of master transcription factors in regulating SE-driven *USP20* expression. (A) IGV plots of CUT&Tag show the signals of H3K27ac, ATAC, and TFs in the *USP20* gene locus super-enhancer in the T-ALL cell line (J.gamma1). (B) The activity of the E3 luciferase reporter was assessed in the T-ALL cell lines (Jurkat, J.gamma1) following the knockdown of *RUNX1* and *ETS1* ($n = 3$). (C) mRNA level of *USP20* in the T-ALL cell lines (Jurkat, J.gamma1) following individual master TF knockdown (RUNX1 and ETS1) is shown *via* qRT-PCR

(Fig. S4E). Specifically, elevated expression was noted in the J. gamma1, 6T-CEM, and Molt4 cell lines. Based on clinical data from our center, we analyzed the survival rates of 24 children with low *USP20* expression and 54 children with high *USP20* expression in T-ALL. The results demonstrated a significantly lower survival rate among the high-expression group than the low-expression group, with a statistically significant difference (Fig. 1F). The clinical characteristics of the patients are detailed in Supporting Information Table S8. We investigated the fact that *USP4* deficiency inhibits cell proliferation and increases apoptosis in T-ALL (Fig. S4F−S4J). In conclusion, our study is the first to identify *USP20* as an SE-regulated gene highly expressed specifically in T-ALL. Furthermore, elevated *USP20* expression is associated with poor prognosis in children with T-ALL, highlighting its important pathogenic role.

3.2. Pivotal role of master transcription factors in the regulation of SE-driven USP20 expression

We analyzed publicly available Hi-ChIP data from T-ALL to confirm broad associations between *USP20* enhancers and promoters. These connections are illustrated by connecting lines above the ChIP-seq profiles in Fig. 2A. Within the *USP20*-SE, we identified three candidate component enhancers (E1−E3) as well as a negative control region (Fig. 2A). These candidate enhancers were cloned into the pGL3-promoter luciferase reporter vector and transfected into Jurkat and J.gamma1 cell lines. E3 demonstrated the highest reporter activity, consistent with its high H3K27ac signal (Fig. 2B). Based on these findings, we concluded that the E3 component enhancer is the main active unit of the *USP20* SE. To confirm the transcriptional function of the enhancer component, we utilized CRISPR intervention to specifically repress the *USP20* E3 *cis*-regulatory element using sgRNAs targeting the dCas9/KRAB cluster (Fig. 2C). The sgRNA2, sgRNA4+5, and sgRNA6+7 targeting E3 significantly reduced USP20 protein and *USP*20 mRNA expression (Fig. 2D and E). Inhibition of *USP*20 SE activity led to significant suppression of cell growth when sgRNA-dCas9/KRAB was transfected into Jurkat and J.gamma1 cells; however, transfection with sgRNA alone had no remarkable impact on cell proliferation (Fig. 2F and Supporting Information Fig. S5A). Additionally, we added the data on the effects of inhibiting *USP20* SE activity using sgRNA-dCas9/KRAB on the proliferation and progression of T-ALL *in vivo* (Fig. S5B). The fluorescence signal level in the E3-sgRNA group showed a significant decrease compared to that in the sg-NC group (Fig. S5B).

To further explore the upstream mechanism, we performed a series of CUT&Tag analyses against T-ALL master TFs. The analysis examined the occupancy of these master TFs (*RUNX1*, *ETS1*, *ERG*, *ETV6*, and *ELF1*) in J.gamma1 and 6T-CEM cells, revealing multiple enrichment sites within the SE region of USP20, with enhancer region E3 showing the most significant enrichment (Fig. 3A, Supporting Information Figs. S6 and S7, Tables S9 and S10). To confirm that T-ALL master TFs directly promote *USP20* expression through the SE, we first knocked down *RUNX1* and *ETS1*, two master TFs in T-cell regulation. Next, to assess enhancer activity, the pGL3-promoter vector with the *USP20*-E3 element was transfected into Jurkat and J.gamma1 cells. Consistent with our hypothesis, the knockdown of master TFs significantly decreased *USP20*-E3 luciferase activity compared to control groups (Fig. 3B). Additionally, at the mRNA level, the absence of any of the master TFs (*RUNX1, ETS1*, *ERG*, *ETV6*, and *ELF1*) consistently and significantly downregulated *USP20* expression (Fig. 3C, Supporting Information Fig. S8A). Besides, overexpression of *RUNX1* and *ETS1* increases the expression of *USP20* (Fig. S8B−S8E). An analysis of expression data from the samples of patients with T-ALL in the GEO database (GSE13159, GSE26713) showed a significant positive correlation between the expression levels of *USP20* and the master TFs *RUNX1* and *ETS1* (Fig. 3D). These results suggest that master TFs *RUNX1* and *ETS1* cooperatively regulate *USP20* transcription by directly occupying its SE regions in T-ALL.

3.3. USP20 knockdown inhibited T-ALL proliferation and progression in vitro and in vivo

To investigate the role of USP20 in T-ALL, *in vitro* experiments were conducted by transfecting three T-ALL cell lines (Jurkat, J. gamma1, and Molt4) with *USP20*-targeting shRNA (sh-*USP20*#1, sh-*USP20*#2, and sh-*USP20*#3) and control shRNA (sh-NC). Significant decreases in USP20 protein and *USP*20 mRNA expression levels were observed in cells transfected with *USP*20 shRNA (#2 and #3) compared to the control group, as determined *via* Western blot and qRT-PCR analyses (Fig. 4A and B). The colony-forming ability of T-ALL cells was significantly reduced following *USP20* knockdown in a soft agar assay (Supporting Information Fig. S9A). PI staining demonstrated that *USP20* knockdown caused cell cycle arrest, resulting in a significant increase in G2/M phase cells while decreasing G1/S phase cells, thereby inhibiting cell proliferation (Fig. S9B). Furthermore, the *USP20* knockdown group exhibited a considerable decrease in cell proliferation compared to the sh-NC group ($P < 0.001$) (Fig. 4C). Additionally, the *USP20* knockdown group exhibited significant growth restriction leading to cellular death compared to the sh-NC group (Supporting Information Fig. S10A). Apoptosis was assessed *via* flow cytometry, showing that *USP20* deficiency induced apoptosis in Jurkat, Molt4, and J.gamma1 cell lines (Fig. 4D and Fig. S10B). Consistent with these findings, Western blot analysis revealed downregulation of *USP20* expression followed by the cleavage of apoptotic proteins PARP, caspase-3 (Fig. 4E), and caspase-8 (Fig. S10C). Besides, overexpression of *USP20* increased *USP*20 mRNA and USP20 protein expression and enhanced cell proliferation *in vitro* (Fig. S10D−S10F). *In vivo*, the effect of *USP20* knockdown was examined by intravenously injecting J.gamma1 cells transfected with sh*USP20* or sh-NC into NSG mice through the tail vein after tagging the cells with luciferase (Fig. 4F). The fluorescence signal level in the sh-*USP20* group showed a significant decrease compared to that in the sh-NC group (Fig. 4G and H). Fluorescence imaging of liver, spleen, and bone samples from mice revealed a substantial decrease in tumor burden in the *USP20* knockdown group compared to that in the control group (Supporting Information Fig. S11A). Survival analysis indicated a substantial median

analysis ($n = 3$). (D) Transcript levels of *USP20*, *RUNX1*, and *ETS1* show a strong positive correlation in T-ALL cases (GSE13159 $n = 165$, GSE26713 $n = 117$), as indicated by a scatter plot. Data are presented as mean ± SD; non-significant (ns), $*P < 0.05$, $**P < 0.01$, $***P < 0.001$, and $****P < 0.0001$.

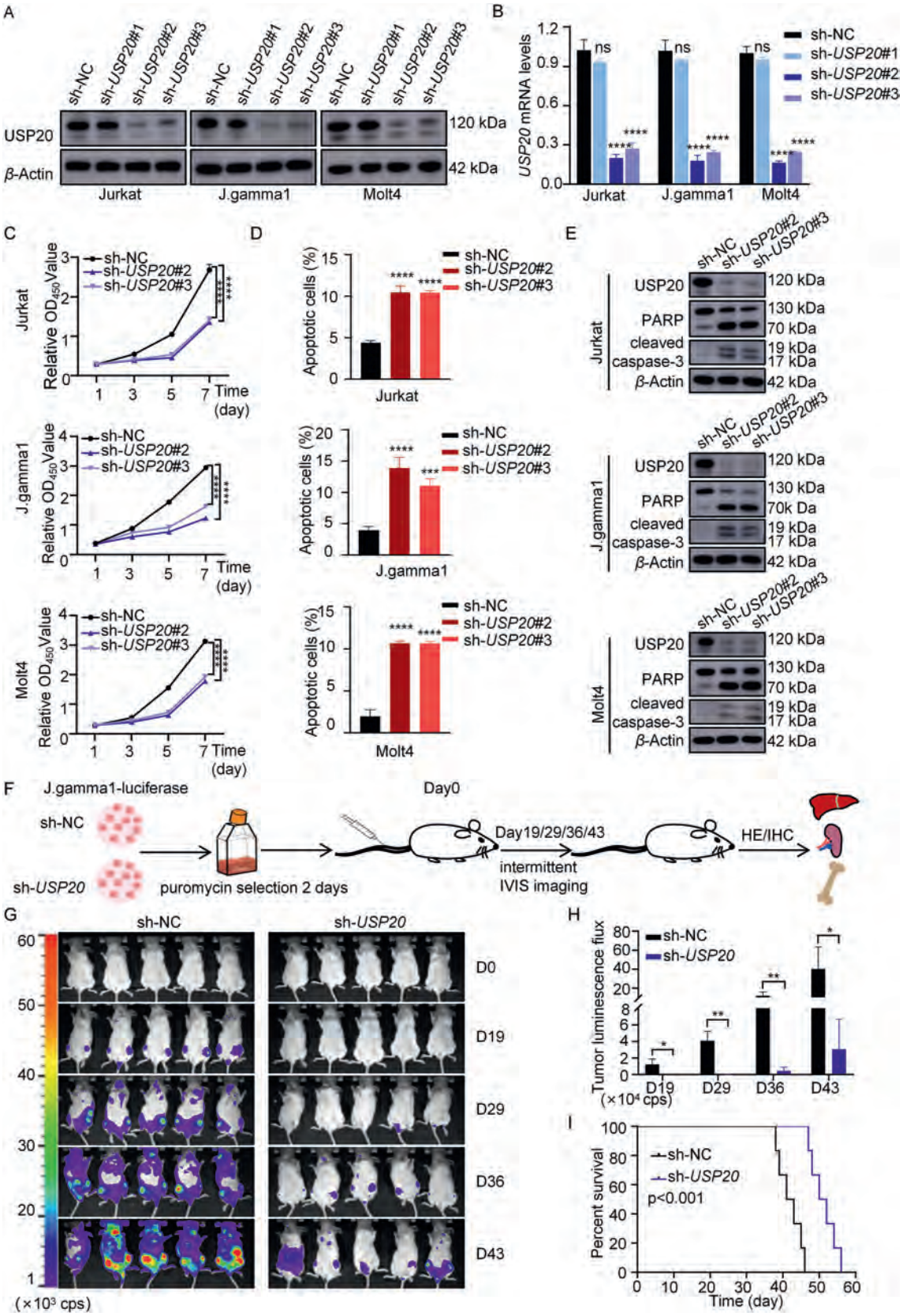

Figure 4 *USP20* knockdown inhibited T-ALL proliferation and progression *in vitro* and *in vivo*. (A) Western blotting verified the *USP20* knockdown levels in the cells. (B) In Jurkat, Molt4, and J.gamma1 cells infected with sh-NC, sh-*USP20*#2, and sh-*USP20*#3, the levels of *USP20* mRNA were measured using qRT-PCR ($n = 3$). (C) The CCK-8 assay was used to calculate the cell proliferation rates of Jurkat, Molt4, and J. gamma1 cells following *USP20* knockdown ($n = 3$). (D) Using flow cytometry, the apoptotic levels in infected Jurkat, Molt4, and J.gamma1 cells

survival advantage for the sh-*USP20* mice (Fig. 4I). The sh-*USP20* group exhibited a marked decrease in the proportion of bone, liver, and spleen $CD45^+$ cells (Fig. S11B), while white light photos of liver and spleen from both groups were obtained (Fig. S11C). No noticeable loss of body weight was observed in the mice of either group (Fig. S11D). Moreover, H&E staining of mouse liver, spleen, and bone marrow revealed a marked decrease in tumor cells in the *USP20* knockdown group compared to controls (Fig. S11E). IHC staining for Ki67 further supported these findings, demonstrating an inhibitory effect on tumor development within the liver, spleen, and bone marrow following *USP20* knockdown (Fig. S11F). In conclusion, the consistent outcomes from both *in vitro* and *in vivo* investigations demonstrate that USP20 knockdown exerts an anti-tumor effect against T-ALL. *In vitro* experiments within a T-ALL mouse model (L1210) indicated that *Usp20* knockdown significantly inhibited T-ALL cell proliferation while increasing apoptosis rates (Supporting Information Fig. S12A−S12D).

3.4. USP20 inhibitor GSK2643943A inhibited T-ALL proliferation and progression in vitro and in vivo

The chemical structure of GSK2643943 is demonstrated in Supporting Information Fig. S13A. Shanghai Sijie Biomedicine Co., Ltd. has identified small-molecule compounds with high affinity for binding to the USP20 protein through virtual screening (Fig. S13B). The results demonstrate that GSK2643943 exhibits a strong affinity for USP20, supporting its potential as a candidate inhibitor targeting USP20 (Fig. S13C). The small-molecule inhibitor of USP20, GSK2643943A, has demonstrated the ability to inhibit cell proliferation and induce apoptosis. When applied at various concentration gradients, GSK2643943A exhibited strong inhibitory effects on four T-ALL cell lines and two normal $CD8^+$ T cell samples, as evidenced by their respective cell viability curves and IC_{50} values shown in Fig. 5A. The effect of GSK2643943A on the proliferation of $CD34^+$ cells is added in Supporting Information Fig. S14A. Additionally, a dose-dependent reduction in c-Myc expression was observed, along with increased cleavage of PARP and caspase-3 in the Jurkat, 6T-CEM, and J.gamma1 cell lines following GSK2643943A treatment (Fig. 5B). Notably, there were no changes in the levels of USP20 protein expression. Furthermore, flow cytometry analysis indicated a dose-related increase in apoptotic cells upon GSK2643943A treatment (Fig. 5C, Fig. S14B). GSK2643943A also caused cell cycle arrest by increasing the proportion of T-ALL cell lines in the G2 phase while decreasing those in the G1 phase, as demonstrated by PI staining (Fig. 5D and Fig. S14C). To investigate the anti-neoplastic function of GSK2643943A in mice, a T-ALL mouse model was established using J.gamma1 luciferase cells (Fig. 5E). When GSK2643943A was administered to mice, the fluorescent signal intensity was significantly lower than that in the control group (Fig. 5F and G). Additionally, in mice treated with GSK2643943A, infiltration of the liver, spleen, and bone marrow was notably reduced compared to that in the control group (Supporting Information Fig. S15A and S15B). A comparison of survival times between the two groups revealed that the GSK2643943A group had a prolonged lifespan (Fig. 5H). Furthermore, there was a significant decrease in the percentage of $CD45^+$ cells in the bone marrow, liver, and spleen in the GSK2643943A treatment group compared to that in the control (Fig. 5I and Fig. S15C). White light photographs of the liver and spleen from mice in both groups were obtained (Fig. S15D), showing no statistically significant difference in body weight between the groups (Fig. S15E). After dissecting the mice to obtain samples from their liver, spleen, bone marrow, intestine, and kidney, HE staining revealed a significant reduction in tumor cells within the liver, spleen, and bone marrow in the GSK2643943A-treated group (Fig. S15F). Notably, no obvious pathological changes were observed in the kidney post-treatment, and intestinal damage appeared less severe (Supporting Information Fig. S16A). The lack of significant variations in body weight among all participants tested indicated that GSK2643943A caused minimal damage to their organs. Moreover, there was a significant reduction in Ki67-positive cells within the livers, spleens, and bone marrow of those treated with GSK2643943A (Fig. S15G). In conclusion, GSK2643943A inhibited the proliferation and progression of T-ALL similarly to USP20 knockdown, both *in vitro* and *in vivo*. With established T-ALL treatment guidelines, we selected cytarabine (Ara-C), glucocorticoids (dexamethasone), etoposide (VP-16), anthracycline (daunorubicin), and GSK2643943A for a combination tria[33]. Experimental results showing how GSK2643943A works with other chemotherapeutic agents failed to show synergy (Fig. S16B).

3.5. Analysis of the molecular mechanisms of USP20 inhibition on proliferation and progression in T-ALL cells

Using J.gamma1 control shRNA and *USP20*-knockdown cells, we performed RNA-seq analysis to identify possible downstream genes regulated by USP20 in T-ALL (Supporting Information Table S11). In the *USP20*-knockdown group, 588 genes were downregulated and 502 genes were upregulated (log_2FoldChange >1.0, FDR <0.05) (Fig. 6A). Gene set enrichment analysis (GSEA) with Hallmark signatures revealed significant enrichment for hypoxia, glycolysis, and MYC-target genes in the *USP20*-knockdown and control groups (Fig. 6B and C, Supporting Information Table S12). Following *USP20* knockdown, a heatmap displayed the expression levels of genes involved in the MYC, hypoxia, and glycolysis pathways (Fig. 6D). A qRT-PCR study demonstrated that following *USP20* knockdown, the expression levels of genes involved in the MYC, hypoxia, and glycolysis pathways, such as *ODC1*, *LDHA*, and *PGK1*, were significantly reduced (Fig. 6E). Additionally, c-Myc protein levels were downregulated following *USP20* knockdown in J.gamma1, Jurkat and Molt4 (Fig. 6F and Supporting Information Fig. S17A). *MYC* mRNA levels were downregulated following *USP20* knockdown in Jurkat and Molt4 (Fig. S17B). MYC-target genes are crucial for T-ALL survival[34]. There is a close relationship between

were determined ($n = 3$). (E) Western blot analysis revealed upregulation of PARP and cleaved caspase-3 in T-ALL cells following *USP20* knockdown. (F) Schematic diagram depicting the experimental design. (G) Relevant luminescence images for the *USP20* knockdown group and the control group were obtained on days 0,19, 29, 36, and 43. (H) Histogram showing the bioluminescence signal values at various times for the two mouse groups ($n = 5$). (I) The sh-*USP20*-treated group showed longer survival than the control group ($n = 6$). Data are presented as mean ± SD; non-significant (ns), $*P < 0.05$, $**P < 0.01$, $***P < 0.001$, and $****P < 0.0001$.

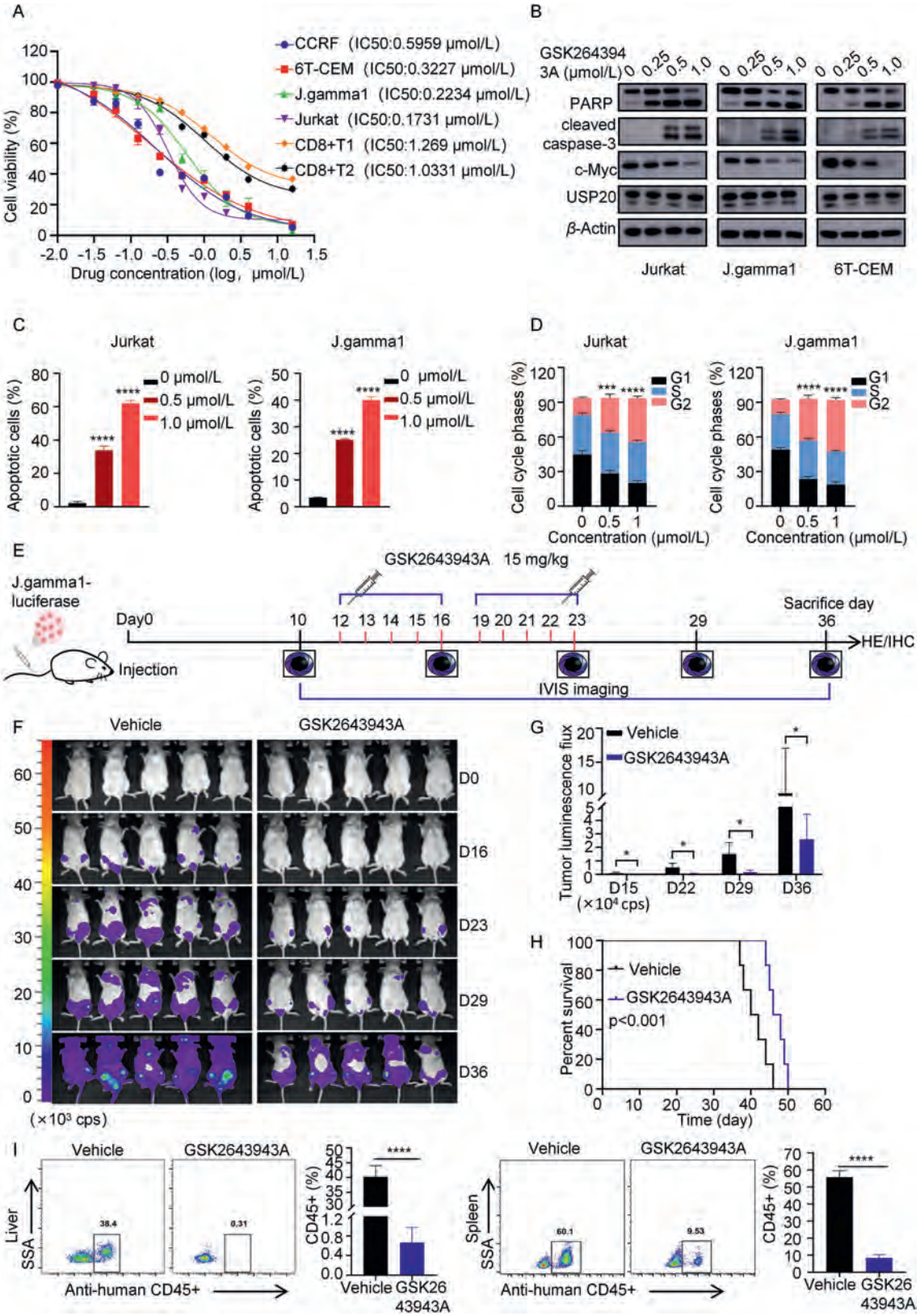

Figure 5 The USP20 inhibitor GSK2643943A inhibited T-ALL proliferation and progression *in vitro* and *in vivo*. (A) Effects of GSK2643943A in T-ALL cells and T cells were detected using CCK-8 assays, which revealed robust inhibition of tumor cell growth in all three T-ALL cell lines ($n = 3$). (B) Western blot analysis showed that PARP, cleaved caspase-3, and C-MYC proteins were stressed in Jurkat, 6T-CEM, and J.gamma1 cells after GSK2643943A treatment, while USP20 protein levels remained unchanged. (C) Flow cytometry demonstrated that GSK2643943A treatment induced more apoptotic cells in a dose-dependent manner in Jurkat and J.gamma1 ($n = 3$). (D) Application of GSK2643943A in Jurkat

hypoxia and glycolytic pathways. Under hypoxic conditions, cells regulate gene expression by activating hypoxia-inducible factors, which promote genes involved in the glycolytic pathway. This pathway produces ATP and metabolites to sustain cell survival and function under hypoxic conditions. T-ALL cells are highly proliferative with increased demands for energy and metabolites, therefore, both the hypoxia and glycolytic pathways play important roles in maintaining tumor cell survival and proliferation[35].

3.6. USP20 promoted the progression of T-ALL by deubiquitinating modified HIF1A and regulating gene transcription through HIF1A

Using mass spectrometry and software analysis, 16 potential target proteins of USP20, including HIF1A, PLK1, and CTNNB1, were identified (Supporting Information Table S13). Among these targets, HIF1A and CTNNB1 stood out based on unique peptides, coverage, and intensity (Fig. 7A and Supporting Information Fig. S18A−S18C). By combining RNA-seq data with a literature review, we focused on the relationship between USP20 and HIF1A. Overexpressing *USP20* in Jurkat and J.gamma1 cells revealed interactions between USP20 and HIF1A or CTNNB1 *via* Co-IP experiments (Fig. 7B and Supporting Information Fig. S19A). Furthermore, knockdown of *USP20* in Jurkat, J. gamma1, and 6T-CEM cells resulted in a significant reduction of HIF1A or CTNNB1 protein levels, while mRNA levels remained unaffected (Fig. 7C and D, Fig. S19B and S19C). Additionally, the USP20 inhibitor GSK2643943A led to a concentration-dependent decrease in HIF1A or CTNNB1 protein levels (Fig. S19D). We hypothesize that USP20 stabilizes HIF1A by regulating its ubiquitination. This was supported by the observation that the proteasome inhibitor MG-132 reversed the downregulation of HIF1A post-*USP20* knockdown in Jurkat and J.gamma1 cells (Fig. 7E), indicating proteasomal degradation of HIF1A. Further evidence comes from our findings that *USP20* knockdown in Jurkat and J. gamma1 cells accelerated HIF1A degradation following cycloheximide (CHX) treatment, whereas *USP20* overexpression prolonged its half-life (Fig. 7F, Fig. S19E and S19F). These results suggest that USP20 stabilizes HIF1A by inhibiting its proteasomal degradation. As USP20 functions as a deubiquitinating enzyme, it is hypothesized that USP20 maintains the stability of HIF1A by inhibiting K48-linked polyubiquitination. To assess the impact of USP20 on HIF1A ubiquitination levels, we overexpressed *USP20* in Jurkat and J.gamma cells, respectively. Our findings indicate that the forced expression of *USP20* significantly reduces k48-linked polyubiquitination associated with HIF1A (Fig. 7G). Besides, Flag-NC, Flag-*USP20*, GFP-*HIF1A*, and *Ub* (wild-type), *Ub-K48* (containing only lysine 48 on the Ub molecule), and *Ub-K63* (containing only lysine 63 on the Ub molecule) were co-expressed in HEK293FT cells. Western blot assays revealed high ubiquitination of HIF1A protein in cells (Supporting Information Fig. S20, lane 1), while *USP20* overexpression markedly reduced HIF1A ubiquitination (Fig. S20, lane 2). Furthermore, overexpression of *USP20* significantly decreased K48-linked polyubiquitination on HIF1A compared to K63-linked polyubiquitination (Fig. S20, lanes 3 and 4). These results suggest that USP20 stabilizes HIF1A by inhibiting K48-linked polyubiquitination. Furthermore, we conducted CUT&Tag experiments to analyze the regulatory roles of USP20 and HIF1A in T-ALL (Supporting Information Fig. S21A and S21B, Supporting Information Tables S14 and S15). USP20 binding sites in J. gamma1 cells significantly overlapped with HIF1A sites (Fig. 8A and B), further validating that *USP20* can regulate gene transcription through *HIF1A*, affecting key genes such as *SLC2A1*, *PER1*, *CIC*, *MAZ*, *PKM*, *CASP9*, and *DLG4* (Fig. 8C, Fig. S21C).

4. Discussion

T-ALL is a highly aggressive hematologic malignancy prone to chemoresistance and relapse. Refractory T-ALL has a survival rate of $<10\%$. Factors, such as genetic mutations, immunophenotypic heterogeneity, treatment resistance, dysregulation of apoptosis, bone marrow microenvironment, and specific patient factors (including age, gender, and genomic traits), contribute to its poor prognosis. Abnormal gene activation or inactivation (*e.g.*, *NOTCH1*, *MYC*, *TAL1*) and pathways (Notch, Wnt/β-catenin, NF-κB) cause T-cell abnormalities and promote T-ALL progression[34,36,37]. Understanding the pathogenesis of T-ALL and discovering new targeted therapies is crucial.

Several studies have demonstrated the involvement of SEs in solid tumors and blood cancers, with their composition and function evolving throughout tumorigenesis. Genes driven by SEs are crucial targets for cancer therapies. In this study, we conducted an in-depth exploration of SE function in T-ALL. Meanwhile, the role of SEs in various other tumor types has also drawn considerable interest. For instance, the Holliday junction recognition protein (*HJURP*) plays a role in tumor formation by protecting chromosome stability. In multiple myeloma with t (4;14) positivity, *HJURP* overexpression, a SE driver gene, promotes proliferation and inhibits apoptosis, making it a promising therapeutic target[18]. Similarly, sphingosine kinase 1 is a key enzyme in the sphingosine pathway, catalyzing the generation of sphingosine-1-phosphate with pro-survival and pro-proliferative functions. In hepatocellular carcinoma, SE drives the aberrant activation of sphingosine kinase 1, contributing to the high expression of this gene, which accelerates the growth and malignant transformation of cancer cells[17]. Targeting the SE complex holds potential for hepatocellular carcinoma treatment. *HOXB8* is a member of the HOX gene family and is thought to promote self-renewal of cancer cells by regulating cell cycle and cell proliferation-related genes. The oncogenic effects of *HOXB8* in colorectal cancer are also driven by SEs, whose aberrant activation results in sustained expression of the gene, thereby driving tumor initiation and

and J.gamma1 cells resulted in changes to the cell cycle profile as measured by PI staining ($n = 3$). (E) Schematic diagram of the experimental design. (F) Bioluminescence imaging on Days 0, 16, 23, 29, and 36 revealed differences between the GSK2643943A group and the vehicle group ($n = 5$). (G) Histograms showing the bioluminescence signal values at various times for the two mouse groups ($n = 5$). (H) The GSK2643943A group showed longer survival compared to the untreated group ($n = 6$). (I) Compared to untreated samples, the number of human CD45-positive cells in the liver and spleen was greatly reduced after treatment with GSK2643943A ($n = 3$). Data are presented as mean ± SD; non-significant (ns), $*P < 0.05$, $**P < 0.01$, $***P < 0.001$, and $****P < 0.0001$.

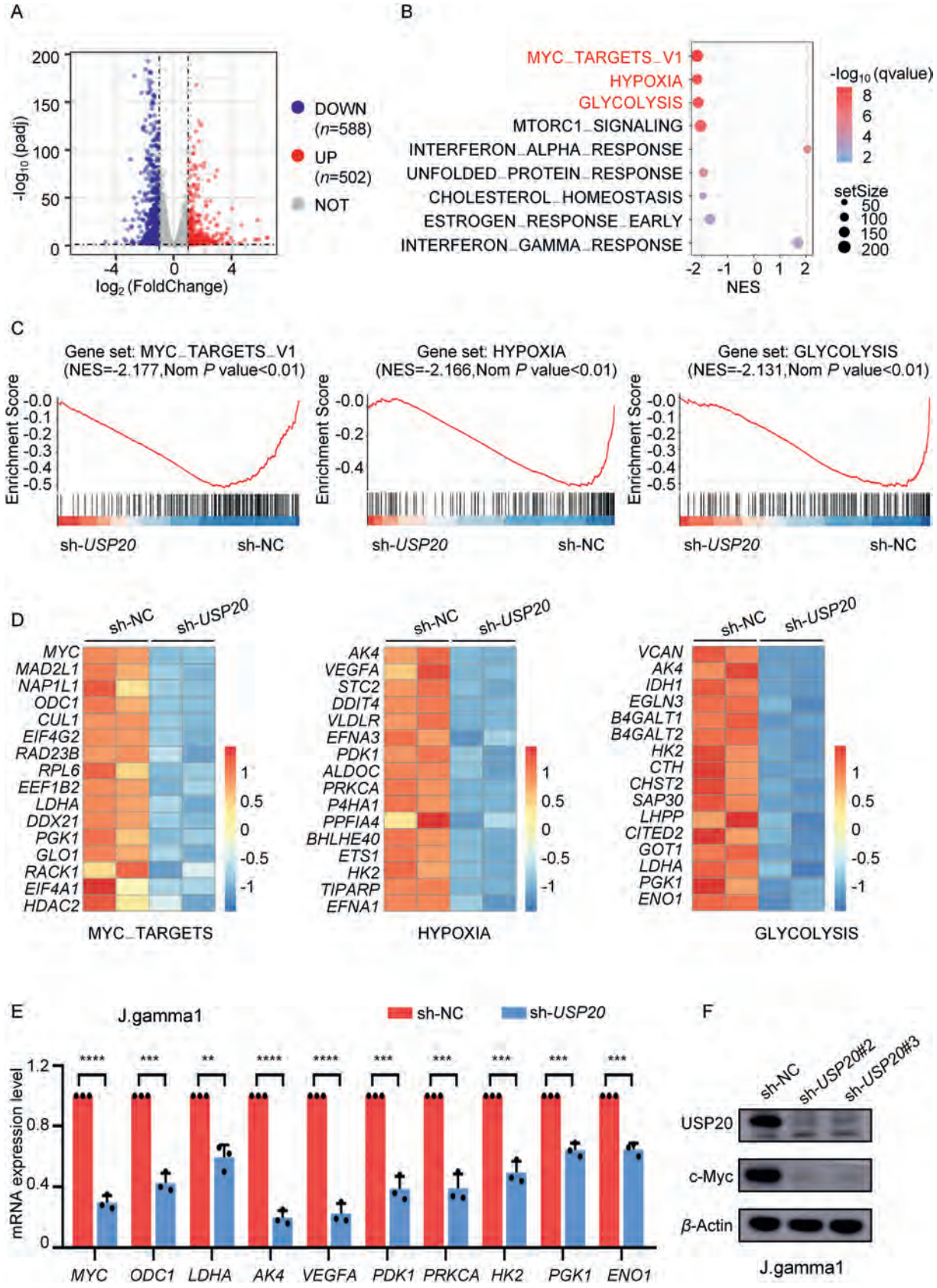

Figure 6 Analysis of the molecular mechanisms of *USP20* inhibition on proliferation and progression in T-ALL cells. (A) Genes from RNA-seq data that were differentially expressed between the *USP20* knockdown and untreated groups were found using a volcano plot analysis; upregulated and downregulated genes are represented by red and blue, respectively. (B) KEGG pathway enrichment study. (C) GSEA plots

progression[15]. We also found that the expression level of the SE-regulated gene *TTC8* was significantly upregulated in NB, which activates the MAPK pathway and promotes the onset and progression of NB, making *TTC8* a potential therapeutic target. *LYL1*, a transcription factor, promotes carcinogenesis by regulating the differentiation and proliferation of hematopoietic stem cells. *ANP32B*, by modulating the pathways of apoptosis inhibition and DNA damage repair, enhances the adaptability of tumor cells to harsh environments and promotes cancer progression. Meanwhile, we have found that *LYL1* and *ANP32B* genes are also regulated by SEs in AML to promote AML progression[27,28]. Taken together, aberrant activation of genes driven by SEs is a key mechanism for the development of multiple tumors, and targeting these SEs and their downstream regulated genes may be an effective therapeutic strategy for multiple cancers.

Sanda et al. identified the crucial roles of SE-related oncogenes T-cell lymphoma invasion and metastasis 2, *IRF4*, and *TP73* in ATL[22-24]. Mansour et al. highlighted a SE triggering *TAL1*'s significance in T-ALL[25], with recent studies further exploring the role of SE-driven *TAL1* in T-ALL[26]. These collective studies underscore the importance of SE-driven genes as potential therapeutic targets in T-ALL. Our research delves into the functions and mechanisms of SE-driven genes in T-ALL. Using H3K27ac ChIP-seq analysis of six T-ALL cell lines and seven T-ALL pediatric samples, we identified *USP20* as the most frequently occurring member of the USP family linked to SE and particularly strongly expressed in T-ALL, based on the CCLE database and BloodSpot. Comparative analysis with $CD34^+$ HSC ChIP-seq and GSE data revealed significant overexpression of *USP20* in T-ALL *versus* normal myeloid cells, particularly $CD34^+$ HSCs. While previous studies have highlighted the significance of *USP7* in T-ALL[6], our data revealed its presence within SEs in cell lines but not in patient samples, confirmed across patient data from GEO. Additionally, other SE-regulated USP family members, such as *USP5*, *USP36*, *USP44*, and *USP49*, are implicated in various tumors[38]. Our study identified *USP20*, *USP44*, and *USP4* as SE-regulated genes in T-ALL. *USP44* has been clearly studied in T-ALL[8]. A study reveals an important regulatory function of *USP4* in HSC regeneration and leukemia progression[39], consistent with our findings that knockdown of *USP4* suppresses proliferation and promotes apoptosis in T-ALL. We therefore focused on *USP20* and demonstrated its significant role in T-ALL pathogenesis. Clinical data from our center further emphasize the correlation between high *USP20* expression and poor prognosis in pediatric T-ALL, suggesting its potential as a treatment target and prognostic marker. Additionally, our investigation into CUT&Tag data of T-ALL cell lines unveiled *RUNX1* and other upstream regulatory genes of *USP20*, a novel finding yet to be reported.

USP20 plays a crucial role in regulating protein stability through various signaling pathways and is involved in important biological processes, such as the cell cycle, proliferation, and apoptosis[4]. Recent research has also highlighted its involvement in non-tumor diseases, including antiviral immunity, metabolic disorders, and neurological conditions[31]. USP20 interacts with vesicle-associated membrane protein-associated proteins to deubiquitinate and stabilize reticulophagy regulator 1 in specific endoplasmic reticulum areas, promoting reticulophagy[40]. Additionally, it regulates autophagy in HECT and RLD domain-containing E3 ubiquitin protein ligase 2-related neurodevelopmental disorders[41]. Furthermore, *USP20* is implicated in various cancers, promoting breast, lung, and colon cancer while inhibiting gastric cancer and ATL[4]. In T-ALL, our study revealed that knockdown of *USP20* reduced cell colony development and proliferation while enhancing apoptosis and prolonging mouse survival in a T-ALL mouse model, suggesting a promoting role for USP20 in T-ALL. The USP20 inhibitor GSK2643943A has shown promising results by reducing fat levels in the liver, blood, and fatty tissue[32] as well as exhibiting anticancer effects by preventing the downregulation of oncolytic herpes simplex virus type 1, strain T1012G viral transmission in an oral squamous cell tumor cell line[42]. Our experiments demonstrated that GSK2643943A increased apoptosis, inhibited proliferation, and prolonged survival in a T-ALL mouse model. Furthermore, histopathological examination of various tissues and changes in body weight suggest minimal toxic side effects of GSK2643943A, making it a viable option for T-ALL clinical treatment. These findings indicate that targeting USP20 could be an excellent approach for T-ALL treatment.

The ubiquitin−proteasome system regulates protein quality control in eukaryotes *via* ubiquitination (catalyzed by E1, E2, E3 enzymes) and deubiquitination (mediated by DUBs). Ubiquitination tags substrates with polyubiquitin chains for proteasomal degradation, while DUBs reverse this by cleaving ubiquitin linkages. The balance between these processes maintains protein homeostasis[43]. The mechanism of USP20 has been the focus of several studies. In cervical cancer, the USP20−p62 pathway affects NF-κB-mediated proliferation, while in breast cancer, USP20 stabilizes extracellular signal-regulated kinase 3 protein, aiding cell migration[4]. β-Catenin was discovered by Wu et al.[44] to be a substrate for USP20, showing its upregulation in various cancers (colon, osteosarcoma, cervical, breast, and colorectal) *via* the Wnt pathway, enhancing cell proliferation, migration, and invasion. Additionally, in esophageal cancer, USP20 stabilizes MCL1 by eliminating its K48 linker ubiquitin chain, leading to chemoresistance and affecting prognosis[45]. Our study investigated the deubiquitinating role of USP20 in T-ALL. We identified sixteen proteins that interact with USP20, including HIF1A and CTNNB1, through mass spectrometry and web-based software analysis. β-Catenin (encoded by CTNNB1), as a known substrate for USP20[44], is essential for MYC enhancer activity, with β-catenin being key to Notch-driven MYC upregulation and a potential target in T-ALL therapy[34]. We confirmed the interaction between USP20 and stabilization of β-catenin through deubiquitination in T-ALL using the Co-IP assay and analysis post-*USP20* knockdown. Consequently, we hypothesize that USP20 regulates MYC

showed that T-ALL cells treated with *USP20* knockdown had gene enrichment in the MYC, hypoxia, and glycolysis signaling pathways. (D) Heatmap showing the expression levels of associated genes in MYC, hypoxia, and glycolysis in J.gamma1 cells treated with *USP20* knockdown. (E) qPCR analysis revealed that the expression levels of related genes, such as *ODC1*, *LDHA*, and *VEGFA*, were decreased. (F) Following *USP20* knockdown in J.gamma1 cells, c-Myc was downregulated in WB analysis. Data are mean ± SD, non-significant (ns), $*P < 0.05$, $**P < 0.01$, $***P < 0.001$, and $****P < 0.0001$.

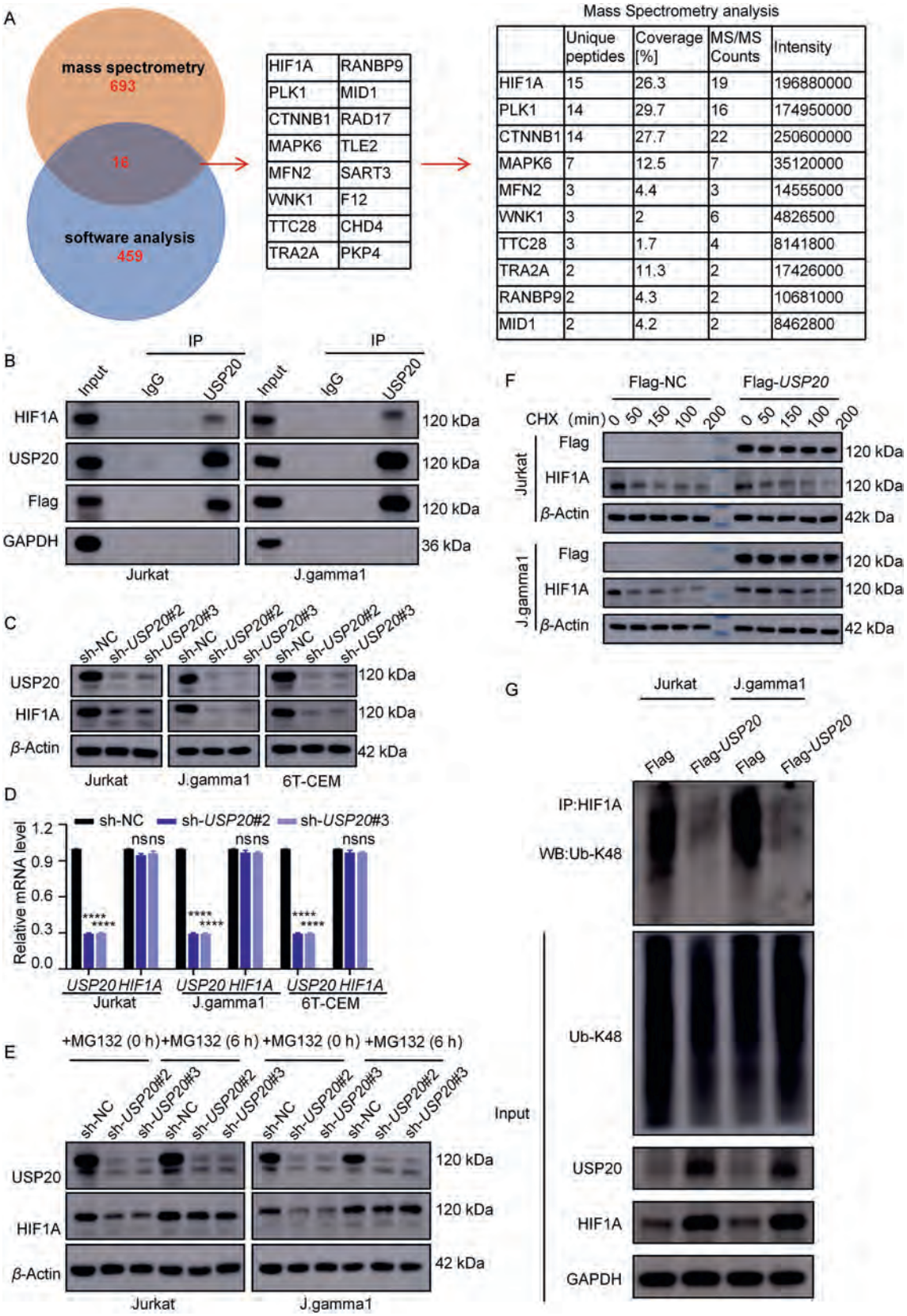

Figure 7 USP20 promotes the progression of T-ALL by deubiquitinating modified HIF1A. (A) Using mass spectrometry and software analysis, 16 potential target proteins of USP20 were identified. The top 10 genes were sorted based on unique peptides, coverage (%), and intensity, with HIF1A leading the list. (B) Western blotting detected USP20, Flag, and HIF1A proteins after immunoprecipitation with the Flag antibody was applied to Jurkat and J.gamma1 cells overexpressing USP20. (C) The amounts of USP20, HIF1A, and β-actin proteins in Jurkat and J.gamma1

via β-catenin, which affects MYC transcription and protein levels, and thus plays an important role in T-ALL. RNA-seq of T-ALL cells after *USP20* knockdown indicated its role in hypoxia pathways. Furthermore, we verified that HIF1A is a substrate for USP20 involved in its proteasome-mediated degradation. Inhibition of USP20 with GSK2643943A reduced HIF1A dose-dependently, confirming it as a substrate for USP20. Our ubiquitination experiments showed that USP20 primarily affects K48-linked polyubiquitination of HIF1A, maintaining its protein stability by inhibiting this modification.

HIF1A serves as a crucial transcription factor in cellular adaptation to hypoxia, regulating genes involved in angiogenesis, glycolysis, cell proliferation, and survival. Hypoxia and genetic alterations are believed to cause its overexpression in many malignancies, where it promotes tumor cell survival and invasion[46]. In a mouse model of T-ALL induced by NOTCH1, the HIF and Wnt/β-catenin signaling pathways synergize to maintain leukemia stem cells[47]. NOTCH1 signaling is essential for HIF1A-induced T-ALL proliferation and invasion[48]. The NOTCH and Wnt/β-catenin pathways are vital regulators in T-ALL, suggesting that the HIF1A pathway also holds significance in T-ALL. Under low oxygen conditions, the HIF1A protein stabilizes, translocates to the nucleus, binds to hypoxia-responsive elements, and triggers downstream gene transcription. Our CUT&Tag analysis of USP20 and HIF1A in J.gamma1 cells revealed their nuclear co-localization and co-regulation of downstream genes, such as glucose transporter 1 (*GLUT1*), period circadian regulator 1 (*PER1*), and capicua transcriptional repressor (*CIC*). IL-7 upregulates GLUT1/solute carrier family 2 member 1 (SLC2A1) in T-ALL cells, enhancing glucose uptake and cell growth[49]. Reduced *O*-GlcNAcylation decreases GLUT1 *via* HIF1A loss, lowering glycolysis and causing endoplasmic reticulum stress[50]. CIC inactivation is crucial in T-ALL[51]. These previously unstudied genes provide valuable insights into the pathogenesis of T-ALL.

Although our study provides new insights into SE-driven *USP20* in T-ALL, we recognize that there are limitations to the study. Our study focused on T-ALL, and further research is needed to determine whether these findings generalize to other cancer types. Future studies should include a wider range of tumor types to validate the broad and specific role of SEs in different cancers. In our follow-up study, we will select eSpCas9 as the high-fidelity Cas9 variant because of its high specificity, extensive validation, and extensive validation. Other commonly used high-fidelity Cas9 variants are HF-Cas9, HypaCas9, Sniper-Cas9, xCas9 and evoCas9. Mismatched sgRNAs can be designed to reduce off-target activity by strategically incorporating nucleotide mismatches at specific positions while maintaining on-target efficiency. Experimental validation methods may include luciferase reporter assays to quantify cleavage efficiency at mismatched targets, genome-wide sequencing to detect rare off-target mutations, or T7 Endonuclease I assays to confirm cleavage at predicted sites. These approaches collectively enable systematic evaluation of CRISPR-Cas9 specificity and refinement of sgRNA design.

L1210 cells are a mouse leukemia cell line derived from lymphoma in DBA/2 mice. Although L1210 cells originate from mouse lymphocytic leukemia rather than T-ALL, they recapitulate critical features of human T-ALL, such as rapid proliferation, impaired apoptosis, and comparable drug sensitivity. These shared characteristics, along with their utility in studying broader leukemia mechanisms (*e.g.*, drug resistance and immune evasion[52]), establish L1210 as a valuable experimental model for T-ALL research. So far, our research has only conducted *in vitro* experiments and lacks *in vivo* studies. In future studies, we will optimize the *in vivo* experimental design.

While GSK2643943A is a recognized USP20 inhibitor, its detailed pharmacological mechanisms remain poorly characterized in the literature. Currently, no studies report its synergistic effects with chemotherapy agents such as cytarabine, dexamethasone, etoposide, or daunorubicin; furthermore, there are no investigations into the interactions between these four chemotherapy drugs and USP20. We speculate that several factors may contribute to the absence of observed synergistic effects between GSK2643943A and the tested chemotherapy drugs. These factors could include drug−drug interactions, competition at target sites, or differing pharmacological mechanisms. USP20 is a deubiquitinase that plays a crucial role in maintaining protein stability by removing ubiquitin chains from target proteins. It regulates signaling pathways associated with cell proliferation, metabolism, and apoptosis, including HIF-1α, AMPK, and mTOR. GSK2643943A acts as an inhibitor of USP20, leading to increased ubiquitination of target proteins, promoting their degradation. This may interfere with the efficacy of chemotherapy drugs that depend on these pathways. GSK2643943A might compete with chemotherapeutic agents (*e.g.*, daunorubicin) for CYP450-mediated metabolism, potentially altering their pharmacokinetics, efficacy, or toxicity profiles. Inhibition of USP20 may alter the stability of cell cycle regulatory proteins, thereby affecting the sensitivity of chemotherapy agents (such as etoposide) to specific phases of the cell cycle. In summary, GSK2643943A may attenuate synergistic interactions with chemotherapy agents by disrupting signaling pathways related to USP20 as well as metabolic pathways or target mechanisms. However, it should be noted that our current findings are preliminary. Future studies are needed to comprehensively investigate the synergistic effects and underlying mechanisms between GSK2643943A and clinically used drugs *in vivo*.

cells that stably expressed sh-NC, sh-*USP20*#2, and sh-*USP20*#3 were measured *via* WB analysis. (D) In Jurkat and J.gamma1 cells that stably expressed sh-NC, sh-*USP20*#2, and sh-*USP20*#3, the mRNA levels of *USP20* and *HIF1A* were measured using qRT-PCR ($n = 3$). Data are mean ± SD, non-significant (ns), $^{*}P < 0.05$, $^{**}P < 0.01$, $^{***}P < 0.001$, and $^{****}P < 0.0001$. (E) Twenty micromolar MG-132 was incubated for 6 h with sh-NC, sh-*USP20*#2, and sh-*USP20*#3 stably expressed in Jurkat and J.gamma1 cells. The protein levels of USP20, HIF1A, and β-actin were measured *via* Western blotting. (F) For the specified periods, 100 μg/mL CHX was applied to Jurkat and J.gamma1 cells that either overexpressed USP20 (Flag-USP20) or stably expressed the empty vector (Flag). Afterward, USP20, HIF1A, and β-actin protein levels were assessed using Western blotting. (G) HIF1A was immunoprecipitated from Jurkat and J.gamma1 cells stably expressing empty vector (Flag) or *USP20* overexpression (Flag-*USP20*), respectively, followed by Western blotting of the precipitated proteins with the antibody specifically for k48-linked ubiquitin (Ub-k48).

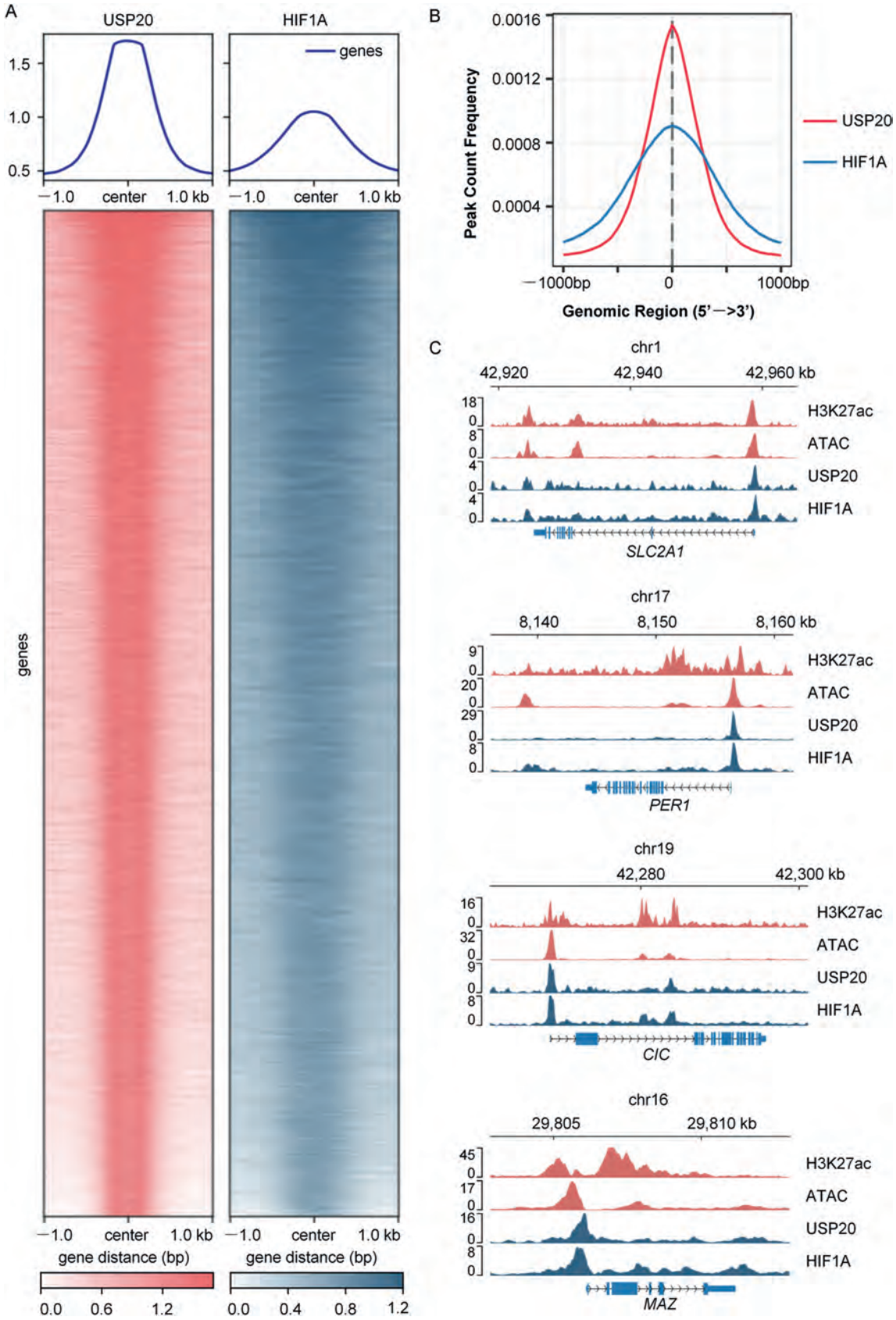

Figure 8 USP20 regulates gene transcription through HIF1A. (A) A heatmap produced by CUT&Tag research revealed that USP20 and HIF1A were occupied in the J.gamma1 cell line. (B) Distribution of HIF1A and USP20 peaks within a ±1000 bp window of USP20 binding sites. (C) CUT&Tag IGV graphs displaying the H3K27ac signal, ATAC signal, and gene locus signal for USP20 and HIF1A in the T-ALL cell line (J. gamma1), highlighting potential target genes, such as *SLC2A1*, *PER1*, *CIC*, and *MAZ*.

5. Conclusions

We identified *USP20* as an SE-regulated gene that exhibits high expression and plays a crucial role in T-ALL. USP20 stabilizes the HIF1A protein by removing its K48-linked polyubiquitinated chain through its deubiquitinating enzyme activity. Additionally, USP20 and HIF1A co-localize with genes, such as *GLUT1*, *PER1*, and *CIC*, to promote T-ALL progression. The specific inhibitor of USP20, GSK2643943A, demonstrates anti-tumor effects similar to those observed with *USP20* knockdown in T-ALL with fewer side effects. Therefore, GSK2643943A represents a potential candidate for T-ALL therapy, highlighting USP20 as a promising target in T-ALL treatment.

Acknowledgments

This work was supported by grants from the National Key R&D Program of China (2022YFC2502700); National Natural Science Foundation (82072767, 82141110, 82172840, 82203442, 82300182, and 82373414, China); Natural Science Foundation of Jiangsu Province (BK20220047, China); Jiangsu Province's Science and Technology Support Program (Social Development) project (BE2021657 and BE2022732, China); Suzhou Health Talent Training Project (GSWS2020047, GSWS2021028 and GSWS2022062, China); the Science and Technology Development Project of Suzhou City (SKY2022170 and SKY2023192, China); Jiangsu Provincial Health Commission Scientific Research Project (Z2022031, M2022102, ZD2022056 and H2023106, China); Medical Research Project of Jiangsu Provincial Health and Family Planning Commission (Key Project ZD2021006, China) and National Outstanding Youth Cultivation Program Project (YYJQ004, China).

Author contributions

Ling Xu: Writing − review & editing, Writing − original draft, Visualization, Validation, Supervision, Software, Resources, Project administration, Methodology, Investigation, Formal analysis, Data curation. Zimu Zhang: Formal analysis, Data curation. Juanjuan Yu: Supervision, Methodology. Tongting Ji: Software, Methodology, Investigation. Jia Cheng: Software. Xiaodong Fei: Supervision, Methodology. Xinran Chu: Formal analysis. Yanfang Tao: Software. Yan Xu: Supervision, Software. Pengju Yang: Resources, Project administration, Investigation. Wenyuan Liu: Software. Gen Li: Methodology. Yongping Zhang: Methodology. Yan Li: Resources. Fenli Zhang: Investigation. Ying Yang: Investigation. Bi Zhou: Methodology. Yumeng Wu: Investigation. Zhongling Wei: Investigation. Yanling Chen: Investigation. Jianwei Wang: Methodology. Di Wu: Supervision. Xiaolu Li: Supervision. Yang Yang: Supervision. Guanghui Qian: Supervision, Methodology. Hongli Yin: Supervision. Shuiyan Wu: Supervision. Shuqi Zhang: Supervision. Dan Liu: Investigation. Jun-jie Fan: Investigation. Lei Shi: Methodology. Xiaodong Wang: Supervision. Shaoyan Hu: Supervision, Investigation, Data curation. Jun Lu: Supervision, Investigation, Funding acquisition, Data curation. Jian Pan: Writing − review & editing, Funding acquisition, Formal analysis, Data curation.

Declaration of competing interest

The authors declare no conflict of interest.

Ethical approval and consent to participate

This study was performed according to The Code of Ethics of the World Medical Association (Declaration of Helsinki) and was approved by the ethics committee of Children's Hospital of Soochow University (No. SUEC2000-021 & No. SUEC2011-037). Written informed consent was obtained from each participating individual's guardian. All animal studies were approved by the Animal Care Committee of Suzhou College (approval number: CAM-SU-AP#: JP-2018-1).

Data availability

Our sequencing and processed data files were submitted to the Gene Expression Omnibus (GEO; http://www.ncbi.nlm.nih.gov/geo/) repository, GSE59657 (Jurkat ChIPseq), GSE76783 (CCRF-CEM ChIP-seq), GSE59657 (MOLT3 ChIP-seq), GSE79288 (MOLT4 ChIP-seq), GSE243772 (PF382 ChIP-seq), GSE18927 (CD3+, CD4+, CD8+T cells ChIP-seq), GSE231486 (CD34+HSC ChIP-seq), GSE267758 (T-ALL1, T-ALL2, T-ALL3, T-ALL4, T-ALL5, T-ALL6, T-ALL7, and J.gamma1 ChIP-seq), GSE165207 (T-ALL Hi-ChIP), GSE267451 (ERG, RUNX1, ETS1, ELF1, ETV6 CUT&Tag) and GSE267258 (J.gamma1 RNA-seq, USP20 and HIF1A CUT&Tag). The mass spectrometry proteomics data have been deposited to the ProteomeXchange Consortium *via* the PRIDE partner repository with the dataset identifier PXD053080. Other relevant data are available from the corresponding authors upon reasonable request.

Appendix A. Supporting information

Supporting information to this article can be found online at https://doi.org/10.1016/j.apsb.2025.07.003.

References

1. Hunger SP, Mullighan CG. Acute lymphoblastic leukemia in children. *N Engl J Med* 2015;**373**:1541−52.
2. Jain N, Lamb AV, O'Brien S, Ravandi F, Konopleva M, Jabbour E, et al. Early T-cell precursor acute lymphoblastic leukemia/lymphoma (ETP-ALL/LBL) in adolescents and adults: a high-risk subtype. *Blood* 2016;**127**:1863−9.
3. Teachey DT, Pui CH. Comparative features and outcomes between paediatric T-cell and B-cell acute lymphoblastic leukaemia. *Lancet Oncol* 2019;**20**:e142−54.
4. Li Q, Ye C, Tian T, Jiang Q, Zhao P, Wang X, et al. The emerging role of ubiquitin-specific protease 20 in tumorigenesis and cancer therapeutics. *Cell Death Dis* 2022;**13**:434.
5. Yi J, Li H, Chu B, Kon N, Hu X, Hu J, et al. Inhibition of USP7 induces p53-independent tumor growth suppression in triple-negative breast cancers by destabilizing FOXM1. *Cell Death Differ* 2023;**30**:1799−810.
6. Shan H, Li X, Xiao X, Dai Y, Huang J, Song J, et al. USP7 deubiquitinates and stabilizes NOTCH1 in T-cell acute lymphoblastic leukemia. *Signal Transduct Target Ther* 2018;**3**:29.
7. Liu S, Xiang Y, Wang B, Gao C, Chen Z, Xie S, et al. USP1 promotes the aerobic glycolysis and progression of T-cell acute lymphoblastic leukemia *via* PLK1/LDHA axis. *Blood Adv* 2023;**7**:3099−112.
8. Chi Z, Zhang B, Sun R, Wang Y, Zhang L, Xu G. USP44 accelerates the growth of T-cell acute lymphoblastic leukemia through interacting with WDR5 and repressing its ubiquitination. *Int J Med Sci* 2022;**19**:2022−32.
9. Whyte WA, Orlando DA, Hnisz D, Abraham BJ, Lin CY, Kagey MH, et al. Master transcription factors and mediator establish super-enhancers at key cell identity genes. *Cell* 2013;**153**:307−19.

10. Kwiatkowski N, Zhang T, Rahl PB, Abraham BJ, Reddy J, Ficarro SB, et al. Targeting transcription regulation in cancer with a covalent CDK7 inhibitor. *Nature* 2014;**511**:616−20.
11. Dowen JM, Fan ZP, Hnisz D, Ren G, Abraham BJ, Zhang LN, et al. Control of cell identity genes occurs in insulated neighborhoods in mammalian chromosomes. *Cell* 2014;**159**:374−87.
12. Dębek S, Juszczyński P. Super enhancers as master gene regulators in the pathogenesis of hematologic malignancies. *Biochim Biophys Acta Rev Cancer* 2022;**1877**:188697.
13. Zhu X, Zhang T, Zhang Y, Chen H, Shen J, Jin X, et al. A super-enhancer controls TGF-beta signaling in pancreatic cancer through downregulation of TGFBR2. *Cell Signal* 2019;**66**:109470.
14. Zhang X, Wang Y, Chiang HC, Hsieh YP, Lu C, Park BH, et al. BRCA1 mutations attenuate super-enhancer function and chromatin looping in haploinsufficient human breast epithelial cells. *Breast Cancer Res* 2019;**21**:51.
15. Ying Y, Wang Y, Huang X, Sun Y, Zhang J, Li M, et al. Oncogenic HOXB8 is driven by MYC-regulated super-enhancer and potentiates colorectal cancer invasiveness *via* BACH1. *Oncogene* 2020;**39**: 1004−17.
16. Chen L, Huang M, Plummer J, Pan J, Jiang YY, Yang Q, et al. Master transcription factors form interconnected circuitry and orchestrate transcriptional networks in oesophageal adenocarcinoma. *Gut* 2020; **69**:630−40.
17. Tsang FH, Law CT, Tang TC, Cheng CL, Chin DW, Tam WV, et al. Aberrant super-enhancer landscape in human hepatocellular carcinoma. *Hepatology* 2019;**69**:2502−17.
18. Jia Y, Zhou J, Tan TK, Chung TH, Chen Y, Chooi JY, et al. Super enhancer-mediated upregulation of HJURP promotes growth and survival of t(4;14)-positive multiple myeloma. *Cancer Res* 2022;**82**: 406−18.
19. Shen JC, Kamath-Loeb AS, Kohrn BF, Loeb KR, Preston BD, Loeb LA. A high-resolution landscape of mutations in the BCL6 super-enhancer in normal human B cells. *Proc Natl Acad Sci U S A* 2019;**116**:24779−85.
20. Zhuo R, Zhang Z, Guo X, Cao H, Chen Y, Tao Y, et al. Super-enhancer-associated TTC8 alters the nucleocytoplasmic distribution of PHOX2B and activates MAPK signaling in neuroblastoma. *Genes Dis* 2023;**10**:1210−3.
21. Chen YL, Li XL, Li G, Tao YF, Zhuo R, Cao HB, et al. BRD4 inhibitor GNE987 exerts anti-cancer effects by targeting super-enhancers in neuroblastoma. *Cell Biosci* 2022;**12**:33.
22. Wong RWJ, Ngoc PCT, Leong WZ, Yam AWY, Zhang T, Asamitsu K, et al. Enhancer profiling identifies critical cancer genes and characterizes cell identity in adult T-cell leukemia. *Blood* 2017;**130**: 2326−38.
23. Wong RWJ, Tan TK, Amanda S, Ngoc PCT, Leong WZ, Tan SH, et al. Feed-forward regulatory loop driven by IRF4 and NF-κB in adult T-cell leukemia/lymphoma. *Blood* 2020;**135**:934−47.
24. Ong JZL, Yokomori R, Wong RWJ, Tan TK, Ueda R, Ishida T, et al. Requirement for TP73 and genetic alterations originating from its intragenic super-enhancer in adult T-cell leukemia. *Leukemia* 2022;**36**: 2293−305.
25. Mansour MR, Abraham BJ, Anders L, Berezovskaya A, Gutierrez A, Durbin AD, et al. Oncogene regulation. An oncogenic super-enhancer formed through somatic mutation of a noncoding intergenic element. *Science* 2014;**346**:1373−7.
26. Smith C, Touzart A, Simonin M, Tran-Quang C, Hypolite G, Latiri M, et al. Harnessing the MYB-dependent TAL1 5′super-enhancer for targeted therapy in T-ALL. *Mol Cancer* 2023;**22**:12.
27. Wan X, Wang J, Fang F, Hu Y, Zhang Z, Tao Y, et al. Super enhancer related gene ANP32B promotes the proliferation of acute myeloid leukemia by enhancing MYC through histone acetylation. *Cancer Cell Int* 2024;**24**:81.
28. Fang F, Lu J, Sang X, Tao YF, Wang JW, Zhang ZM, et al. Super-enhancer profiling identifies novel critical and targetable cancer survival gene LYL1 in pediatric acute myeloid leukemia. *J Exp Clin Cancer Res* 2022;**41**:225.
29. Yu J, Yang Y, Zhou R, Tao Y, Zhu F, Jiao W, et al. The BET inhibitor GNE-987 effectively induces anti-cancer effects in T-cell acute lymphoblastic leukemia by targeting enhancer regulated genes. *Carcinogenesis* 2024;**45**:424−35.
30. Zhang K, Lu J, Fang F, Zhang Y, Yu J, Tao Y, et al. Super enhancer regulatory gene FYB1 promotes the progression of T cell acute lymphoblastic leukemia by activating IGLL1. *J Immunol Res* 2023; **2023**:3804605.
31. Qin B, Zhou L, Wang F, Wang Y. Ubiquitin-specific protease 20 in human disease: emerging role and therapeutic implications. *Biochem Pharmacol* 2022;**206**:115352.
32. Lu XY, Shi XJ, Hu A, Wang JQ, Ding Y, Jiang W, et al. Feeding induces cholesterol biosynthesis *via* the mTORC1−USP20−HMGCR axis. *Nature* 2020;**588**:479−84.
33. Teachey DT, O'Connor D. How I treat newly diagnosed T-cell acute lymphoblastic leukemia and T-cell lymphoblastic lymphoma in children. *Blood* 2020;**135**:159−66.
34. Gekas C, D'altri T, Aligue R, Gonzalez J, Espinosa L, Bigas A. β-Catenin is required for T-cell leukemia initiation and MYC transcription downstream of Notch1. *Leukemia* 2016;**30**:2002−10.
35. Fahy L, Calvo J, Chabi S, Renou L, Le Maout C, Poglio S, et al. Hypoxia favors chemoresistance in T-ALL through an HIF1α-mediated mTORC1 inhibition loop. *Blood Adv* 2021;**5**:513−26.
36. Liau WS, Tan SH, Ngoc PCT, Wang CQ, Tergaonkar V, Feng H, et al. Aberrant activation of the GIMAP enhancer by oncogenic transcription factors in T-cell acute lymphoblastic leukemia. *Leukemia* 2017; **31**:1798−807.
37. Kumar V, Palermo R, Talora C, Campese AF, Checquolo S, Bellavia D, et al. Notch and NF-κB signaling pathways regulate miR-223/FBXW7 axis in T-cell acute lymphoblastic leukemia. *Leukemia* 2014;**28**:2324−35.
38. Dewson G, Eichhorn PJA, Komander D. Deubiquitinases in cancer. *Nat Rev Cancer* 2023;**23**:842−62.
39. Liu B, Zhang X, Zhou Y, Liu H, Wang Z, Fu Y, et al. USP4 regulates ribosome biogenesis and protein synthesis for hematopoietic stem cell regeneration and leukemia progression. *Leukemia* 2024;**38**:2466−78.
40. Zhang M, Wang Z, Zhao Q, Yang Q, Bai J, Yang C, et al. USP20 deubiquitinates and stabilizes the reticulophagy receptor RETREG1/FAM134B to drive reticulophagy. *Autophagy* 2024;**20**: 1780−97.
41. Sala-Gaston J, Perez-Villegas EM, Armengol JA, Rawlins LE, Baple EL, Crosby AH, et al. Autophagy dysregulation *via* the USP20−ULK1 axis in the HERC2-related neurodevelopmental disorder. *Cell Death Discov* 2024;**10**:163.
42. Lu R, Wu G, Chen M, Ji D, Liu Y, Zhou GG, et al. USP18 and USP20 restrict oHSV-1 replication in resistant human oral squamous carcinoma cell line SCC9 and affect the viability of SCC9 cells. *Mol Ther Oncolytics* 2021;**23**:477−87.
43. Fang YZ, Jiang L, He Q, Cao J, Yang B. Deubiquitination complex platform: a plausible mechanism for regulating the substrate specificity of deubiquitinating enzymes. *Acta Pharm Sin B* 2023;**13**: 2955−62.
44. Wu C, Luo K, Zhao F, Yin P, Song Y, Deng M, et al. USP20 positively regulates tumorigenesis and chemoresistance through beta-catenin stabilization. *Cell Death Differ* 2018;**25**:1855−69.
45. Feng J, Liu P, Li X, Zhang D, Lin H, Hou Z, et al. The deubiquitinating enzyme USP20 regulates the stability of the MCL1 protein. *Biochem Biophys Res Commun* 2022;**593**:122−8.
46. Masoud GN, Li W. HIF-1α pathway: role, regulation and intervention for cancer therapy. *Acta Pharm Sin B* 2015;**5**:378−89.
47. Giambra V, Jenkins CE, Lam SH, Hoofd C, Belmonte M, Wang X, et al. Leukemia stem cells in T-ALL require active Hif1alpha and Wnt signaling. *Blood* 2015;**125**:3917−27.
48. Zou J, Li P, Lu F, Liu N, Dai J, Ye J, et al. Notch1 is required for hypoxia-induced proliferation, invasion and chemoresistance of T-cell acute lymphoblastic leukemia cells. *J Hematol Oncol* 2013;**6**:3.
49. Barata JT, Silva A, Brandao JG, Nadler LM, Cardoso AA, Boussiotis VA. Activation of PI3K is indispensable for interleukin

7-mediated viability, proliferation, glucose use, and growth of T cell acute lymphoblastic leukemia cells. *J Exp Med* 2004;**200**:659−69.
50. Ferrer CM, Lynch TP, Sodi VL, Falcone JN, Schwab LP, Peacock DL, et al. *O*-GlcNAcylation regulates cancer metabolism and survival stress signaling *via* regulation of the HIF-1 pathway. *Mol Cell* 2014; **54**:820−31.
51. Simón-Carrasco L, Graña O, Salmón M, Jacob HKC, Gutierrez A, Jiménez G, et al. Inactivation of Capicua in adult mice causes T-cell lymphoblastic lymphoma. *Genes Dev* 2017;**31**:1456−68.
52. Li M, Lu M, Lai Y, Zhang X, Li Y, Mao P, et al. Inhibition of acute leukemia with attenuated *Salmonella typhimurium* strain VNP20009. *Biomed Pharmacother* 2020;**129**:110425.